Analysis Note for Run 5 Charged Pion A_{LL}

Adam Kocoloski

April 7, 2009

1 How We Calculate A_{LL}

Let's start with the equation for a raw double spin asymmetry:

$$A_{LL} = \frac{\sum_{runs} P_Y P_B (N_{++} - R N_{+-})}{\sum_{runs} P_Y^2 P_B^2 (N_{++} + R N_{+-})} \tag{1}$$

where R is a ratio of spin-dependent luminosities determined from the BBC scaler system:

$$R = \frac{\mathcal{L}_{UU} + \mathcal{L}_{DD}}{\mathcal{L}_{DU} + \mathcal{L}_{UD}} \tag{2}$$

Each of the $\mathcal{L}_{ij}$ is a sum of the scaler counts from board 5 for timebins 7, 8, and 9 for events with a given spin state (in terms of 4 bit spin states, UU = 5, DU = 6, UD = 9, and DD = 10). The formula for the statistical uncertainty on A_{LL} neglects uncertainties on the relative luminosities and beam polarizations. Assuming Poisson statistics on N_{++} and N_{+-} we have for a single run

$$\left(\frac{\sigma_{A_{LL}}}{A_{LL}}\right)^2 = \frac{N_{++} + R^2 N_{+-}}{(N_{++} - R N_{+-})^2} + \frac{N_{++} + R^2 N_{+-}}{(N_{++} + R N_{+-})^2} - 2\frac{N_{++} + R^2 N_{+-}}{N_{++}^2 - R^2 N_{+-}^2} \times COV(N_{++} - R N_{+-}, N_{++} + R N_{+-}) \tag{3}$$

where the covariance term is just

$$COV(N_{++} - R N_{+-},\ N_{++} + R N_{+-}) = N_{++} - R^2 N_{+-} \tag{4}$$

In the case of small asymmetries, the relative uncertainty on the numerator dominates the uncertainty on A_{LL}:

$$\left(\frac{\sigma_{A_{LL}}}{A_{LL}}\right)^2 = \left(N_{++} + R^2 N_{+-}\right)\left[\frac{1}{(N_{++} - RN_{+-})^2} + \frac{1}{(N_{++} + RN_{+-})^2} - \frac{2(N_{++} - R^2 N_{+-})}{N_{++}^2 - R^2 N_{+-}^2}\right] \quad (5)$$

$$\approx \frac{N_{++} + R^2 N_{+-}}{(N_{++} - RN_{+-})^2} \quad (6)$$

ROOT's TH1::Divide method does the error propagation correctly in this limit (it ignores the covariance), so we rely on it to calculate the results. The generalization to a sum over runs is straightforward since the yields for each run are uncorrelated.

1.1 Multi-Particle Statistics

In this analysis it's very often the case that we accept multiple pions from a single event. Treating each of these particles as an independent event and simply using $\sqrt{N}$ for the errors as we did in the previous section is not quite correct. Following the prescription in Jim's note on multi-particle statistics we fill each bin in a histogram at most once per event, using a weight equal to the number of particles that fell into that bin. Note that this approach does not account for correlations across bins.

1.2 Background Subtraction

Next we consider asymmetries with sideband subtraction. Specifically, the raw charged pion asymmetries in this analysis are contaminated by protons, kaons, and electrons. The protons and kaons are necessarily combined into a single sideband. Both sidebands have some non-negligible pion contribution. We start by defining a reduced background fraction that accounts for the impurities in the sideband:

$$f_x(y) = \frac{x \text{ counts in } y \text{ window}}{\text{total in } y \text{ window}} \quad (7)$$

$$f'(x) = \frac{f_x(\pi)}{1 - f_\pi(x)} \quad (8)$$

The standard equations for the background-subtracted A_{LL}^{π} and its statistical uncertainty are only modified by replacing the background fraction for each sideband with its reduced background fraction:

$$A_{LL}^{\pi} = \frac{A_{LL}^{\pi,raw} - f'(p+K)A_{LL}^{p+K,raw} - f'(e)A_{LL}^{e,raw}}{1 - f'(p+K) - f'(e)} \quad (9)$$

$$\sigma_{A_{LL}^{\pi}} = \frac{\sqrt{\sigma^2_{A_{LL}^{raw}} + f'(p+K)^2 * \sigma^2_{A_{LL}^{p+K,raw}} + f'(e)^2 * \sigma^2_{A_{LL}^{e,raw}}}}{1 - f'(p+K) - f'(e)} \tag{10}$$

2 Event Selection

We used the File Catalog filter `sanity=1,production=P05if,filename~st_physics,filetype=daq_reco_mudst` and selected runs from the list in Appendix C. We analyzed events triggered by 96201 ("MB"), 96221 ("JP1"), and/or 96233 ("JP2"). The total integrated luminosity included in the analysis works out to 2.1 pb^{-1}.

Events from the MB, JP1, and JP2 trigger samples were selected for further analysis if the time difference between the signals in the two BBCs (a crude measure of the primary vertex position) fell into bins 7, 8, or 9. We used this measurement instead of the position of the TPC vertex to be consistent with the event sample used to measure the relative luminosities. We also required that the offline trigger simulator accepted the event with the same trigger decision as the online trigger. This requirement cuts down on false triggers due to hot towers or other online detector malfunctions.

3 Track Cuts

We identify charged pions as primary tracks from the highest-ranked vertex in the event satisfying the following cuts:

- $p_T > 2.0\ GeV/c$
- $|\eta| < 1.0$
- track has > 25 fit points
- DCA of associated global track to primary vertex < 1.0 cm

The cut on p_T ensures we are in a physics regime describable by perturbative QCD, and enables pion identification via dE/dx measurements in the relativistic rise (more on that later). The cuts on η, number of fit points, and distance of closest approach to the primary vertex are straightforward cuts used to reject poor-quality tracks and tracks from secondary vertices. These latter three cuts are shown in Figure 1.

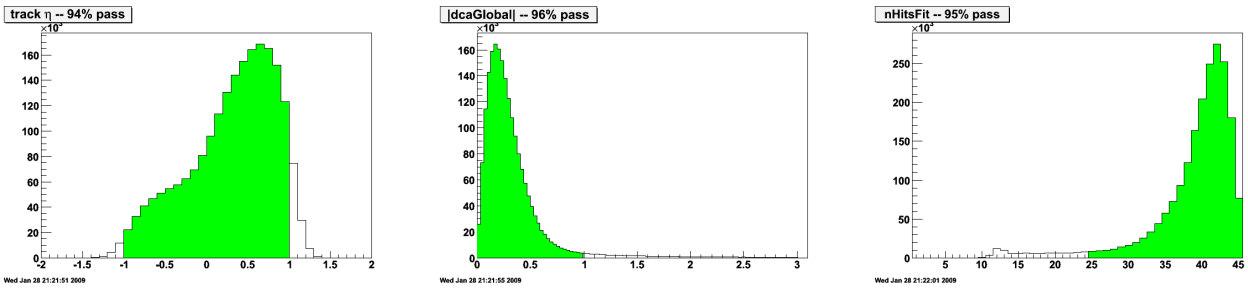

(a) eta cut (b) dca cut (c) nHits cut

Figure 1: Track acceptance and quality cuts.

4 Pion Identification

Charged pions are identified and separated from kaons, protons, and electrons by the amount of energy they lose in the TPC. The dE/dx of a TPC track is obtained by sorting the hits according to energy loss, tossing out the top 30%, and averaging the rest. Track dE/dx values for a given particle species at a fixed momentum are Gaussian, so we can also express the dE/dx value for each track in terms of a deviation from the mean dE/dx for some identified particle at that track's momentum. In particular, track energy loss values at STAR are commonly given in terms of "$n\sigma(\pi)$", the deviation from the mean of the pion peak divided by the width of the pion peak. Protons and kaons fall to the left of the pion peak (lower energy loss) and electrons fall to the right (higher energy loss).

It turns out there is some significant time dependence in the Run 5 $n\sigma(\pi)$ distributions. Rather than assume a fixed mean of 0.0 for the pion Gaussian, I performed a triple Gaussian fit on the $n\sigma(\pi)$ distribution for each fill and extracted time-dependent means to better calibrate the PID cut. More details are on my Drupal blog at PID Stability.

After this recalibration we can extract yields for the various species of charged particles by fitting the $n\sigma(\pi)$ distributions with a multi-Gaussian parametric function. We start with 8 Gaussians – one each for π^+, π^-, K^+, K^-, p, $\bar{p}$, e^+, and e^-. We can reduce the number of free parameters by applying the following constraints:

- all widths must be equal (dE/dx resolution isn't particle-dependent)
- particle/antiparticle pairs should have the same mean
- $\pi - K$, $\pi - p$, and $\pi - e$ separations are known from other analyses – we can use them as input parameters

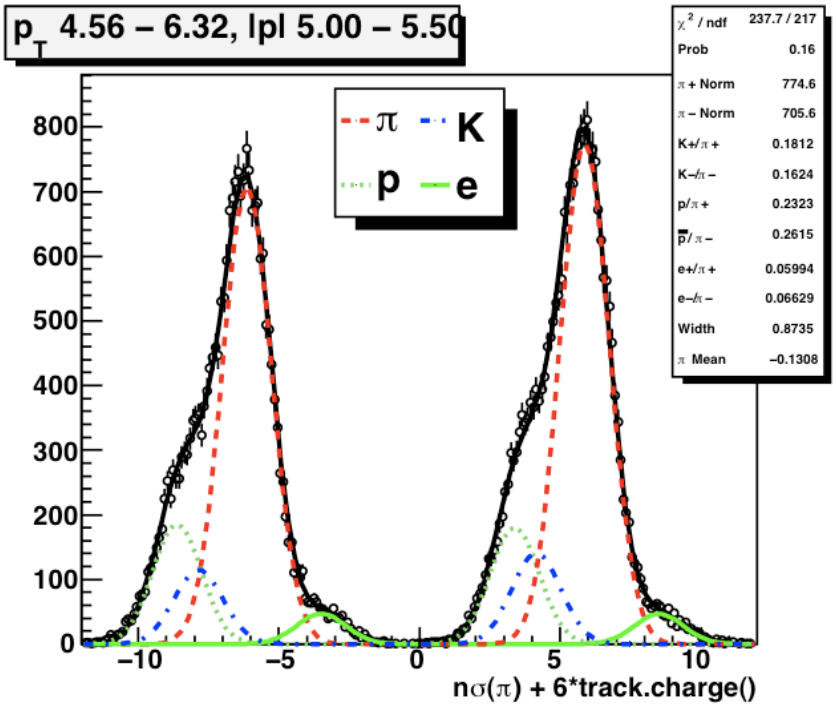

Figure 2: Example PID fit result

In the end we have 24 - 7 - 4 - 3 = 10 free parameters in the fit: the Gaussian width, the mean of the π peak, and the yields. The particle separations change as a function of momentum, not p_T, so we slice each p_T bin into momentum bins and fit each one individually. Figure 2 shows a "typical" fit result. Notice that the tracks have been shifted by 6*track.charge() in order to plot positive and negative charges on the same histogram. The full set of fits is available in Appendix D.

With this database of particle yields in hand we can calculate the set of PID cuts that minimize the statistical uncertainty on the background-subtracted A_{LL} (Equation 10). We wrote a simple minimization routine assuming $\sigma^2_{A_{LL}} = 1/N$ for the raw asymmetries and obtained the results in Table 1.

5 Results

We calculate A_{LL} using Equations 9 and 10. These formulae require raw asymmetries for pions, protons+kaons, and electrons, as well as reduced background fractions in the pion window for the latter two groups. The effect of the background subtraction on the raw pion asymmetries is illustrated in Figure 3.

p_T bin	π window	proton/kaon max	electron min
[2.00 - 3.18]	(-1.10, 2.30)	-2.10	2.60
[3.18 - 4.56]	(-1.40, 2.10)	-2.10	2.40
[4.56 - 6.32]	(-1.40, 1.80)	-2.10	2.40
[6.32 - 8.80]	(-1.40, 1.80)	-2.10	2.40
[8.80 - 12.84]	(-1.30, 1.40)	-2.10	2.10

Table 1: PID Selection Windows

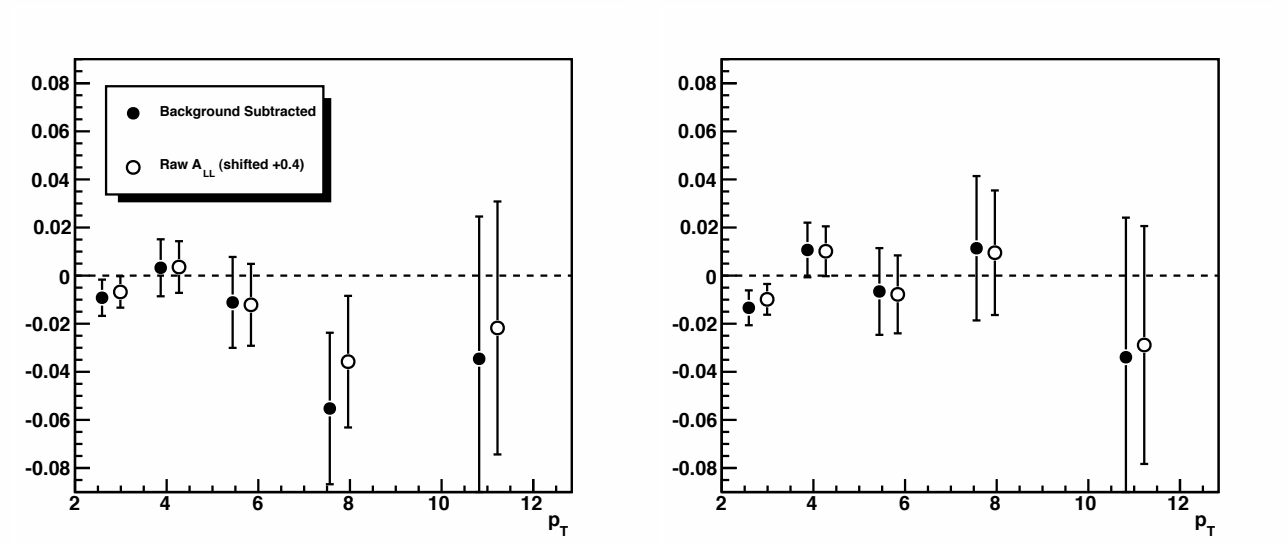

Figure 3: Change in the pion asymmetries due to background subtraction

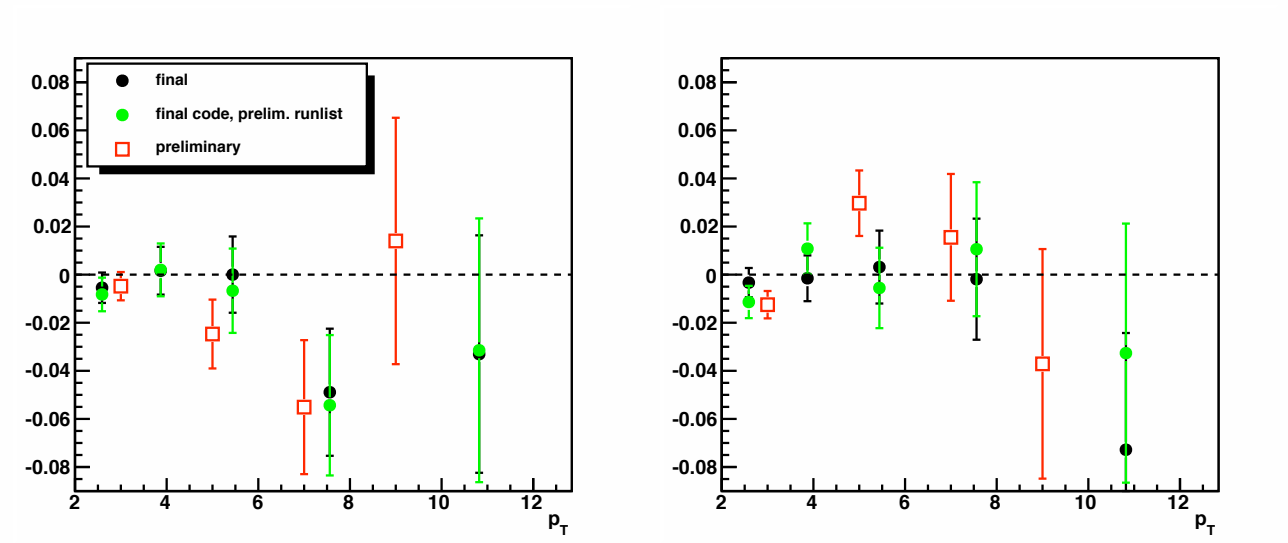

Figure 4: Comparison of preliminary and final asymmetries

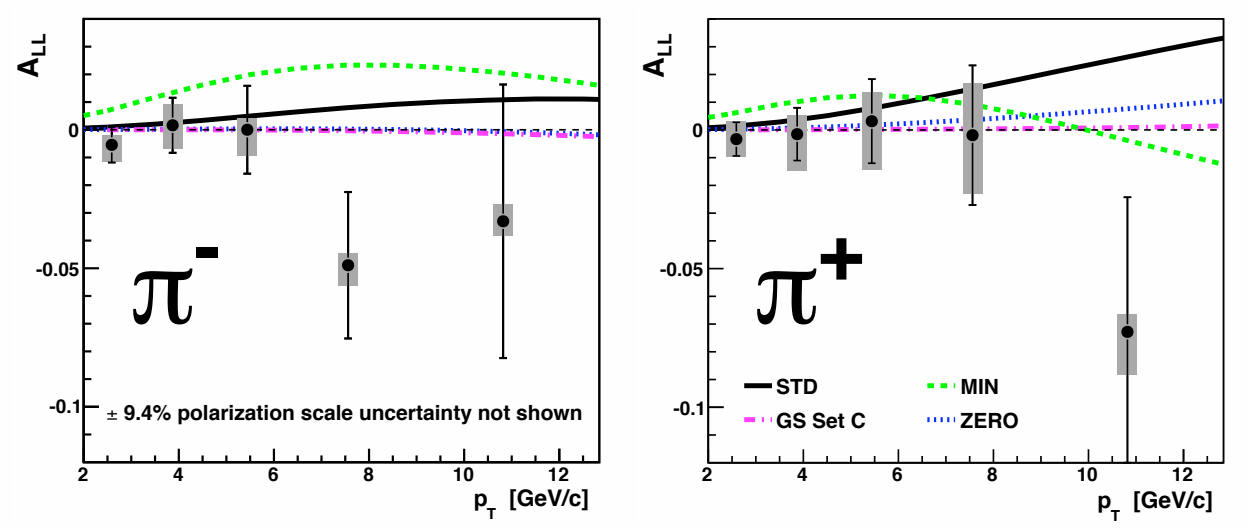

Figure 5: Double Spin Asymmetries for Inclusive Charged Pion Production

The final results in this note differ in several respects from the preliminary results initially presented at SPIN 2006. The runlist has been modified, the data are binned differently, and PID contamination is accounted for by background subtraction instead of assigning a systematic uncertainty. Figure 4 plots the preliminary results, the final results, and an intermediate step where the final code is used on the preliminary runlist.

Figure 5 is STAR's first measurement of A_{LL} for inclusive charged pion production. The data are plotted in bins of pion transverse momentum. The error bars represent statistical uncertainties, and the gray boxes represent asymmetric point-to-point systematic uncertainties summed in quadrature. The data are compared to NLO pQCD calculations convoluted with DSS fragmentation functions.

Further details on the systematic uncertainty evaluations are presented in the following section.

6 Systematic Uncertainties

The dominant systematic uncertainty in this analysis arises from trigger and reconstruction bias. The following subsections address this and other sources of bias in order of their contribution to the total systematic.

6.1 Trigger and Reconstruction Bias

We determine the size of this systematic uncertainty using a leading-order Monte Carlo evaluation of A_{LL}. We start with the kinematics and hard scattering subprocess of each Pythia event and determine numerator

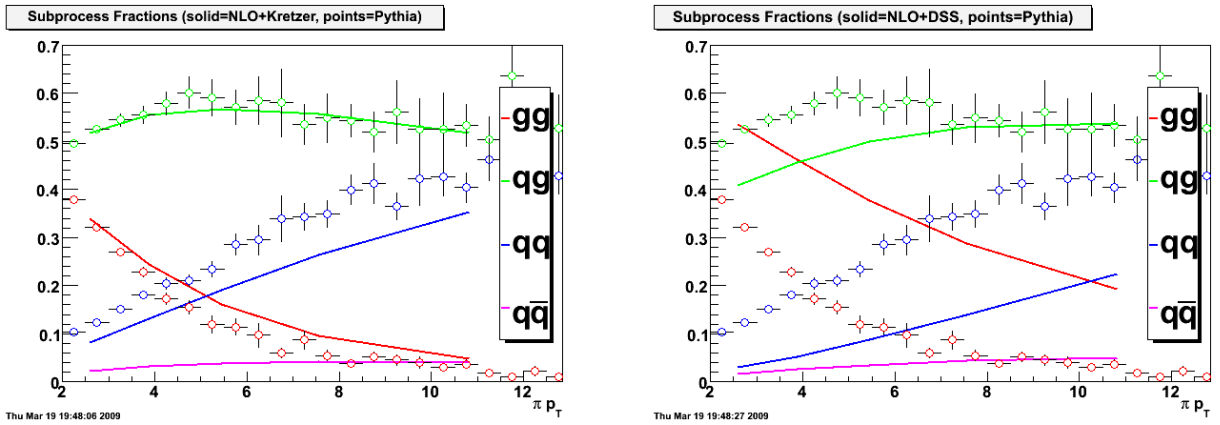

(a) Kretzer (b) DSS

Figure 6: Comparison of subprocess contributions to charged pion production in Pythia and NLO pQCD calculations incorporating two different fragmentation functions. The Pythia results agree much better with the calculations using Kretzer fragmentation functions

and denominator weights by calculating a partonic a_{LL} and sampling from polarized and unpolarized parton distribution functions. We can use these weights to calculate an A_{LL} for any set of simulated events. Specifically, we can measure the difference between the "true" A_{LL} for all Pythia events and the "reconstructed" A_{LL} using only triggered events with reconstructed charged pions and use that to assign the systematic uncertainty.

This procedure obviously requires that our Monte Carlo generator does a good job of reproducing the actual event kinematics. Unfortunately, we have found that the fragmentation tune in Pythia 6.4 is not quite up to the task. In Figure 6 we compare the subprocess contributions to charged pion production reported by Pythia with the results of NLO pQCD calculations incorporating Kretzer and DSS fragmentation functions. The DSS set is known to better describe RHIC kinematics, but in Figure 6 it's clear that Pythia agrees much better with Kretzer.

Getting the subprocess contributions right is an important precondition for using the Method of Asymmetry Weights to evaluate trigger and reconstruction bias, quite simply because A_{LL} has such a strong subprocess dependence. To confirm that the problem is really isolated to Pythia's fragmentation functions, we examined the ratio of pions fragmenting from the quark and the gluon in qg scattering events. That ratio is shown in Figure 7, and confirms that the fragmentation model is Kretzer-like, with much softer gluon fragmentation and/or harder quark fragmentation than we observe at RHIC.

We decided that, rather than plumb the depths of Pythia's independent fragmentation model, we would apply a p_T- and subprocess-dependent reweighting factor to our simulations to generate DSS-like fragmenta-

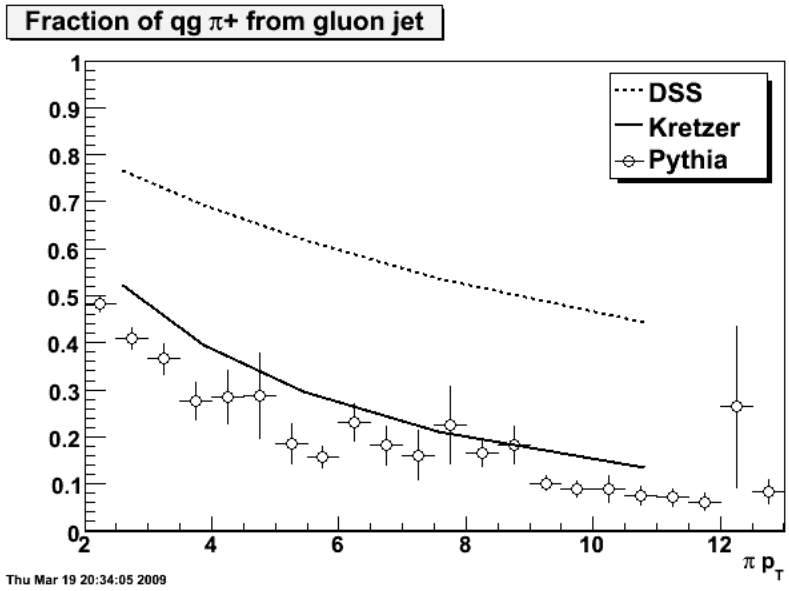

Figure 7: Fraction of pions produced in quark-gluon scattering events that fragment from the gluon. Once again, the Pythia distributions agree much better with the calculation that uses Kretzer fragmentation functions.

tion. The effect of this reweighting is shown in Figure 8. The filled markers show markedly better agreement with the NLO pQCD calculations than the open markers, particularly in scenarios such as GRSV-MIN where the difference in A_{LL} between gg and qg subprocesses is large. The agreement is still not perfect; one might speculate that Pythia gives too much weight to favored quark fragmentation, since at high p_T the π^- asymmetries are too small (indicating a relatively large d quark contribution) and the π^+ asymmetries are too large (consistent with a large u quark contribution). However, as the trigger and reconstruction is not expected to be quark flavor dependent we have decided to press forward with these simulations.

Figure 9 examines the difference between asymmetries for a "true" sample using untriggered events and pions pulled straight from the Pythia record, and a "trigger+reco" sample where the events must satisfy the JP2 trigger simulator and the pion kinematics are obtained from TPC track reconstruction. In some cases, the difference between the two samples is smaller than the uncertainty on the "trigger+reco" sample (see Figure 10). We use the larger of the two to assign the systematic.

The size of the systematic obviously depends on the polarized gluon distributions that are included in the analysis. Previous measurements have excluded the maximal polarization scenarios as well as scenarios with the functional form of the GRSV set and integral gluon polarizations larger than STD. As a result, we use an envelope defined by the GRSV M105 and STD scenarios. The results of this analysis are shown in

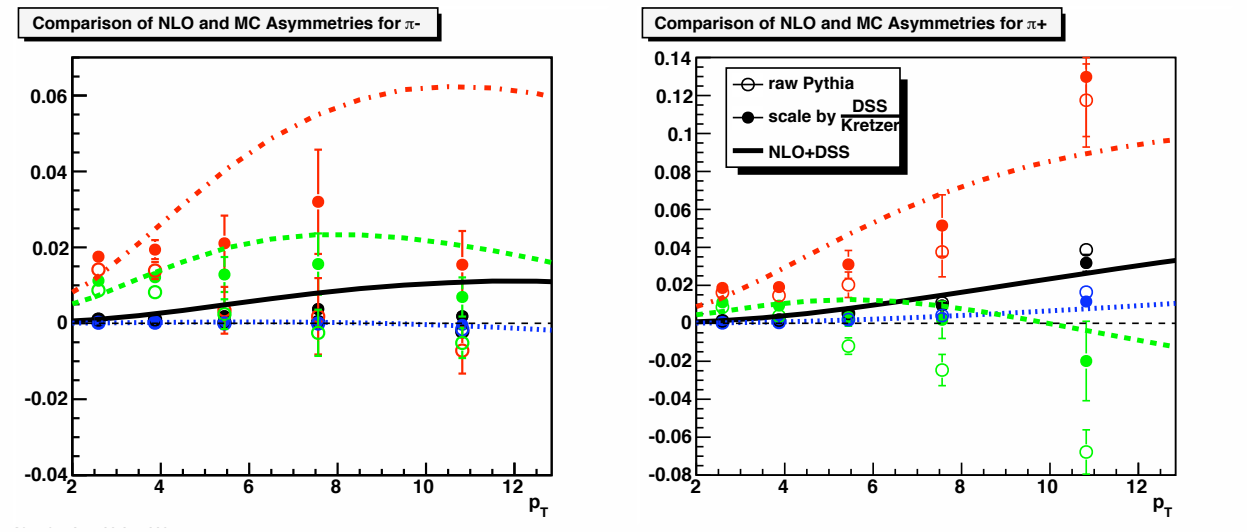

Figure 8: Comparison of Monte Carlo asymmetries with NLO pQCD calculations incorporating DSS fragmentation functions. The open markers show results obtained using STAR's Pythia tune. The filled markers show the change in the asymmetries after reweighting the gg, qg, and qq distributions by the ratio of subprocess fractions calculated using DSS and Kretzer fragmentation functions.

Table 2.

p_T bin	π^- uncertainty	π^+ uncertainty
[2.00 - 3.18]	-0.0059 +0.0027	-0.0061 +0.0061
[3.18 - 4.56]	-0.0083 +0.0072	-0.0128 +0.0066
[4.56 - 6.32]	-0.0093 +0.0034	-0.0176 +0.0101
[6.32 - 8.80]	-0.0072 +0.0036	-0.0209 +0.0186
[8.80 - 12.84]	-0.0048 +0.0057	-0.0152 +0.0062

Table 2: Trigger and Reconstruction Bias Uncertainties

6.2 Beam Polarization Vectors

The beam polarization vectors in Run 5 were determined through an analysis of left-right and up-down asymmetries in the BBC for longitudinal and transverse running. The analysis was performed by Kasia Kowalik (link), who determined the beam angles to be $(\theta, \phi) = (7.9°, 74.0°)$ (Blue) and $(17.2°, 138.7°)$ (Yellow). As the beam polarization vector has non-longitudinal components, a non-zero double-transverse asymmetry A_Σ would contaminate our measured A_{LL} at some small level.

Obtaining an accurate and precise measurement of A_{sigma} for the 2005 run is a challenge. The 2005 transverse running was statistics-starved, and the JP trigger thresholds in the 2006 run are not comparable to 2005. I've elected to simply use a conservative limit on A_Σ of 0.1, flat across p_T. The systematic

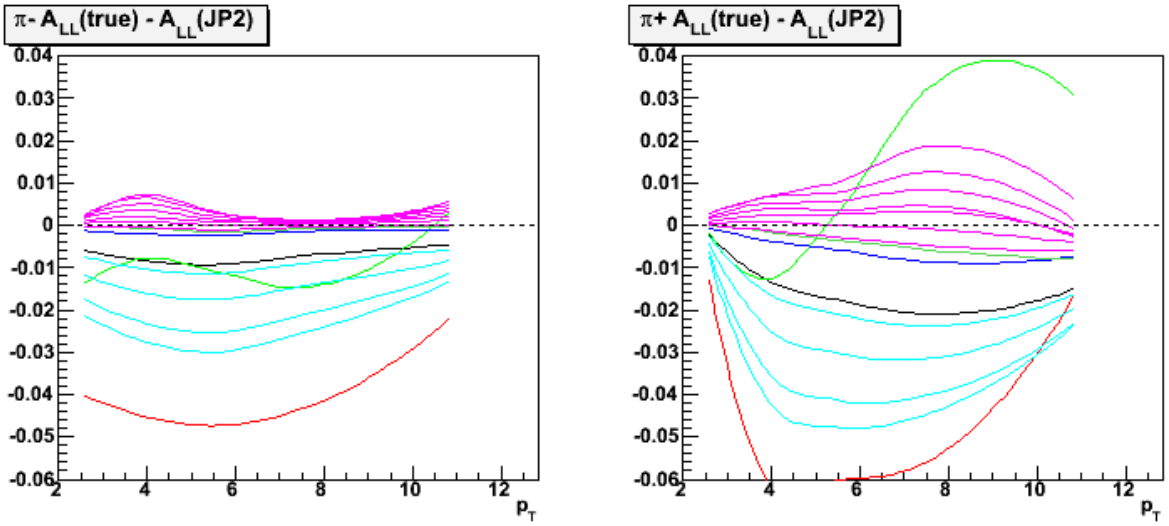

Figure 9: Difference between true and reconstructed Monte Carlo asymmetries after fragmentation reweighting.

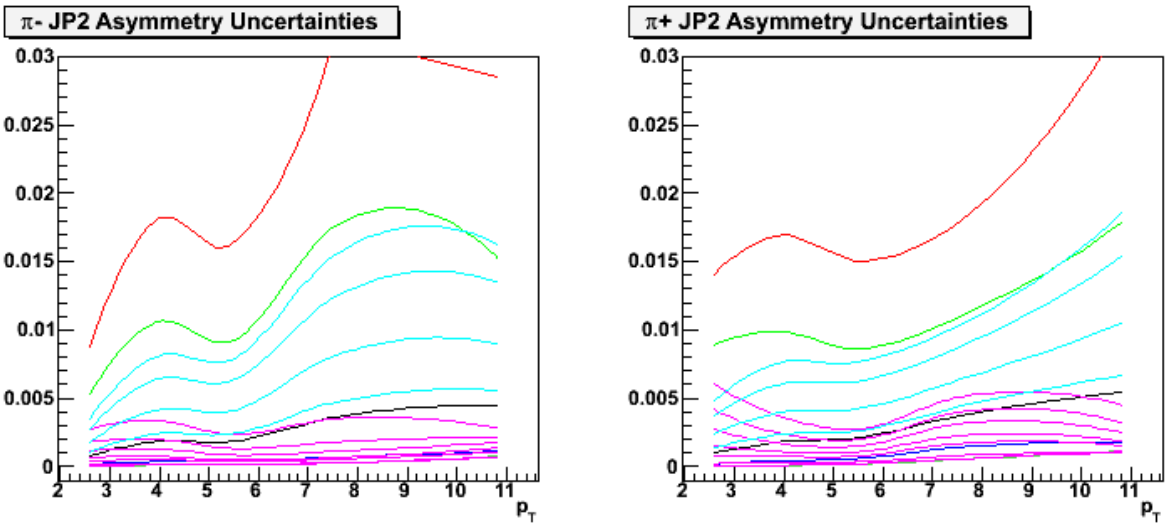

Figure 10: Uncertainty on reconstructed Monte Carlo asymmetries. If the uncertainty is larger than the difference between true and reconstructed asymmetries we use this to assign the systematic instead.

uncertainty on A_{LL} is calculated as

$$\delta A_{LL}^{A_\Sigma}(p_T) = |tan\theta_B tan\theta_Y cos(\phi_Y - \phi_B) A_\Sigma(p_T)| = 0.018 \times |A_\Sigma(p_T)| = 0.0018 \tag{11}$$

6.3 Relative Luminosity Uncertainty

Our statistical uncertainties on A_{LL} assume perfect knowledge of the relative luminosity of the different spin states. This systematic addresses that simplification.

6.3.1 BBC/ZDC Comparisons

Note: analysis by Murad Sarsour

We can quantify the precision with which we understand the relative luminosities in the BBC by using an independent luminosity monitor, the ZDCs. In the absence of non-statistical fluctuations, the uncertainty on R will be dominated by the statistics in the ZDCs, which count at a much lower rate than the BBCs during proton-proton running.

A couple of problems in the ZDC data need to be corrected before a comparison to the BBCs can be trusted. The first problem is due to the "killer bit" algorithm, which suppressed signals in the ZDCs for 10 bunch crossings after an initial signal. The algorithm is used in heavy ion running to prevent ringing in the calorimeters from generating false signals, but in pp running it biases the ZDC counts. Bunch crossings immediately following abort gaps (where the killer bit is more likely to be off) end up with more ZDC counts than crossings in the middle of a filled set of bunches. As a result, the ratio of relative luminosities obtained from the ZDC and BBC will not be flat, see Figure 11.

The procedure developed to correct for this effect requires scaling the counts for a given bunch crossing by a factor that takes into account the frequency with which the previous ten bunch crossings had a signal. For the ZDC singles rates, the formula for the corrected counts n_j in a given bunch crossing j is

$$n_j^{corrected} = n_j * \frac{N_{cycles}}{N_{cycles} - \sum_{i=1}^{10} n_{j-i}} \tag{12}$$

where N_{cycles} is the number of times the beams cycled through STAR in the run. Figure 12 shows the effect of applying the correction for a sample run.

The formula to correct the ZDC coincidence counts is complicated by the need to track the killer bits for the two detectors simultaneously. The formula for the corrected coincidence counts c_j given singles counts

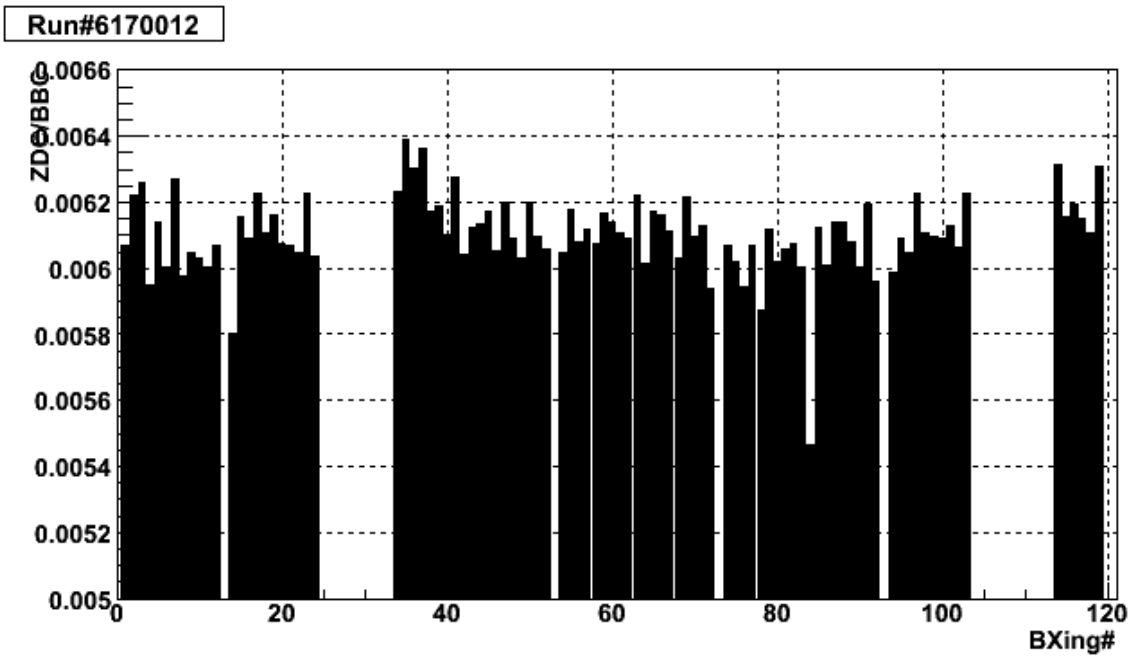

Figure 11: Ratio of ZDC and BBC counts versus bunch crossing. Notice that the ratio is larger in bunch crossings immediately following abort gaps.

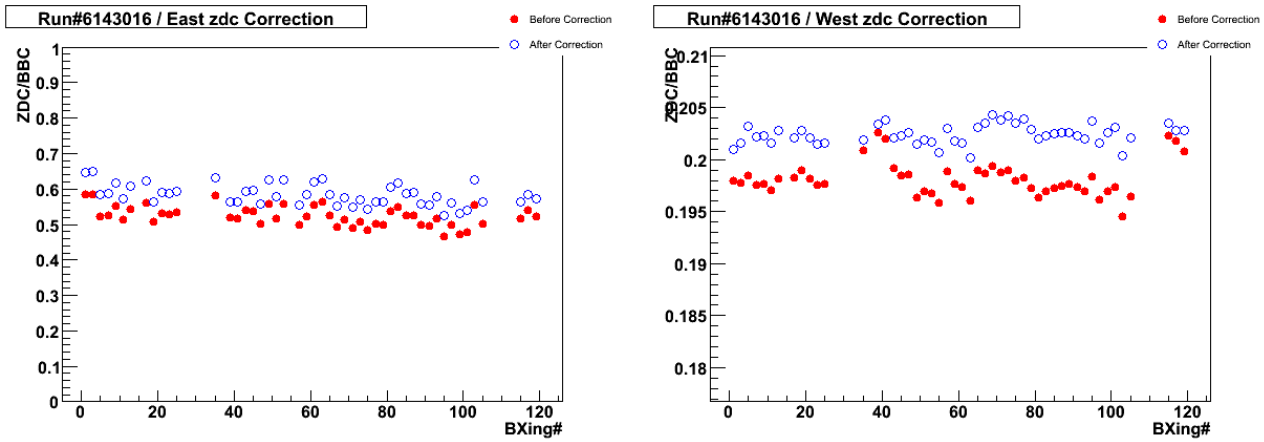

Figure 12: Change in the ZDC singles rates after applying the killer bit correction.

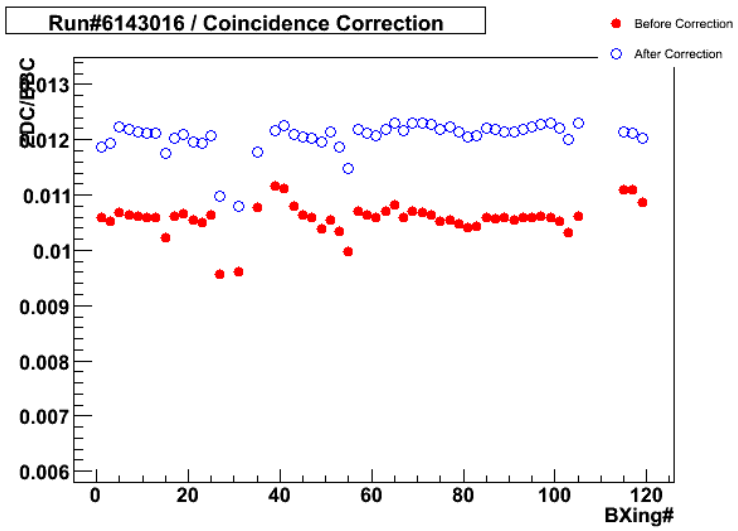

Figure 13: Change in the ZDC coincidence rates after applying the killer bit correction.

e_j (ZCDE) and w_j (ZDCW) is

$$\alpha_j = N_{cycles} - \sum_{i=1}^{10} c_{j-i}$$
$$\beta_j = \sum_{i=1}^{10}(e_j + w_j - 2 * c_j) - \sum_{i=1}^{9}\left[\frac{(e_j - c_j) * (w_j - c_j)}{\alpha_j - (e_{j-10} - c_{j-10})} + \frac{(e_j - c_j) * (w_j - c_j)}{\alpha_j - (w_{j-10} - c_{j-10})}\right] + ...$$
$$c_j^{corrected} = c_j * \frac{N_{cycles}}{\alpha_j - \beta_j} \tag{13}$$

and the effect of the killer bit correction on the coincidence distributions is shown in Figure 13

The second problem that we need to correct has come to be known as the "even-odd" effect. It turns out that the ZDC coincidence rates are often different for even-numbered and odd-numbered bunch crossings. This oscillation can introduce a false asymmetry if it aligns coherently with a particular spin pattern. For instance, in Figure 14 we see that the ZDC coincidence rates are always higher when the spin of the blue beam is down. Figure 15 shows the time dependence of this even-odd oscillation, with the colors now representing individual fills. To quantify the bias this introduces on A_{LL}, we can define the fractional overlap between the even-odd ZDC oscillation and relevant portion of the spin pattern for A_{LL} using a 120 element vector $|EO\rangle = |+1, -1, +1, -1, ...\rangle$ and another 120 element vector $|LL\rangle$ whose elements are 1 if the bunch crossing is UU or DD, -1 if UD or DU, and 0 otherwise. The inner product of these vectors measures the susceptibility of A_{LL} for that spin pattern to any even-odd oscillation.

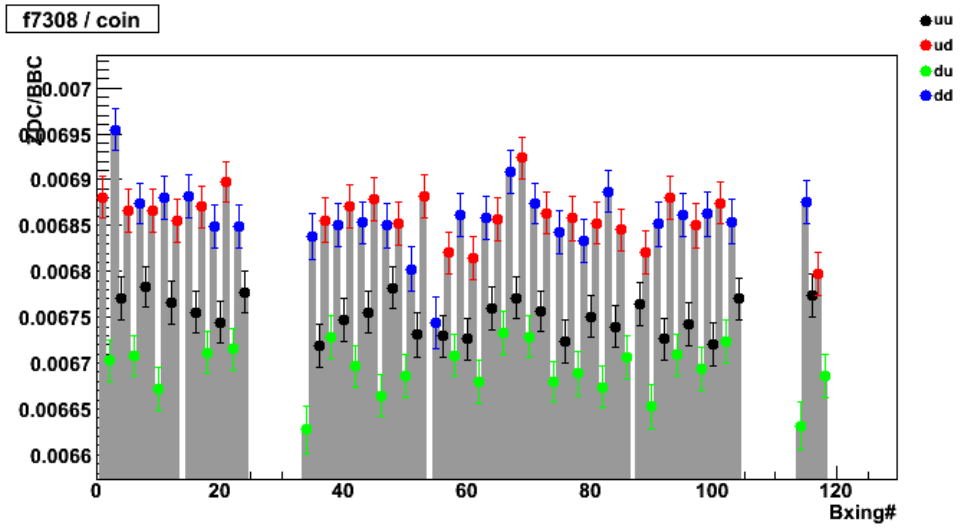

Figure 14: Example of a coherent spin pattern and even-odd ZDC rate oscillation. In this case, the ZDC rate is always higher when the spin of the blue beam is down.

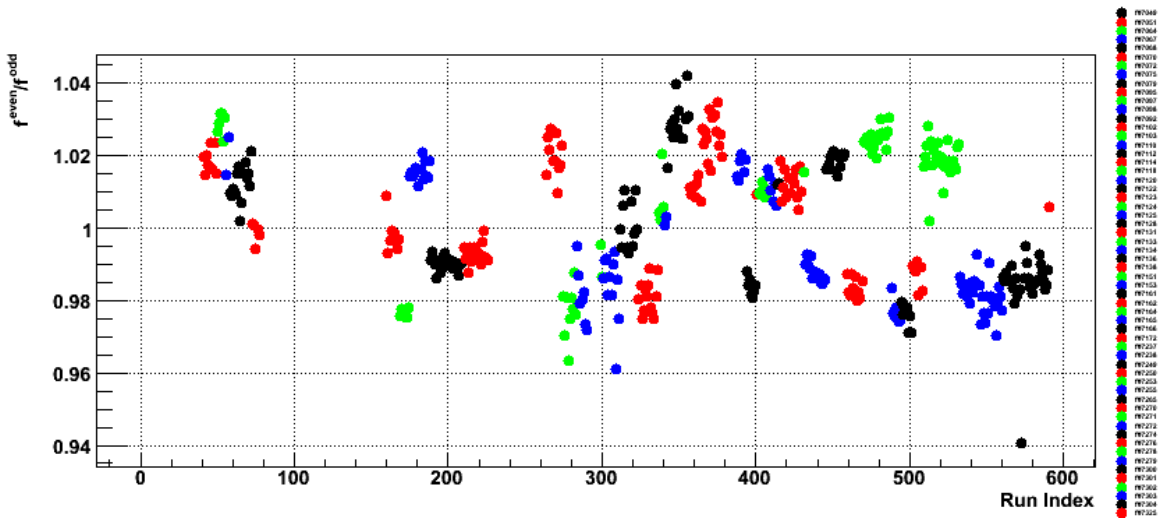

Figure 15: Magnitude of even-odd rate asymmetry versus time.

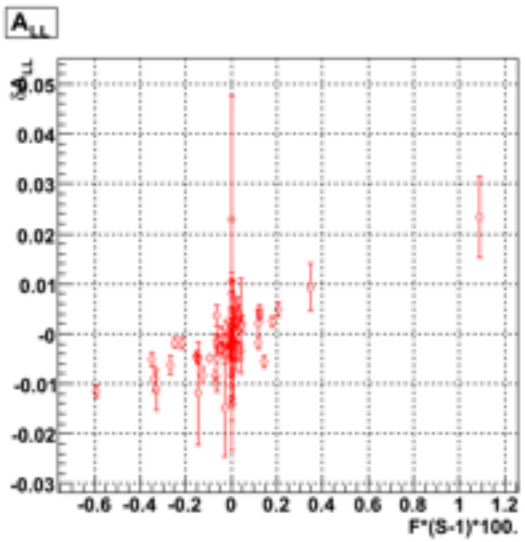

Figure 16: Change in A_{LL} versus the product of the even-odd rate oscillation amplitude and the fractional overlap $\langle EO|LL\rangle$. Deviations from 0 on the x-axis indicate fills where A_{LL} is biased by the even-odd effect.

It turns out that A_{LL} is less biased by the even-odd rate oscillation in the ZDC than, say, the blue beam single-spin asymmetry. Figure 16 plots the fill-by-fill change in A_{LL} if the ZDC is used for relative luminosities instead of the BBC against the the product of the fractional overlap $F \equiv \langle EO|LL\rangle$ and the magnitude of the even-odd oscillation $S-1$. Placing a cut on $|F*(S-1)| < 0.002$ is well-motivated. For fills without reliable ZDC information, we use Figure 15 to assume a conservative $|S-1| = 0.03$.

After correcting for the killer bits and rejecting the fills that fail the even-odd oscillation cut the uncertainty on A_{LL} due to the uncertainty in the relative luminosities is estimated to be 9.32×10^{-4}.

6.3.2 Beam Gas Background

Note: analysis by Kasia Kowalik

The relative luminosities obtained from the BBCs might also be biased by false signals generated by beam-gas background. We can try to quantify this by studying the coincidence rate in crossings where one of the two beams has an unfilled bunch ("abort gaps"). The beam-gas background is assumed to be crossing- and spin-independent, but it can be different in each beam. It follows that the per-crossing coincidence rate due to beam-gas in each beam is just the average number of BBC coincidences found in the abort gaps for that beam. In Figure 17, the x-axis is the background rate divided by the total rate, defined as the average number of coincidences per bunch crossing with a spin state of UU, UD, DU, or DD. The two histograms are incremented for each STAR run. We see that the background rate in the BBCs due to beam-gas is typically

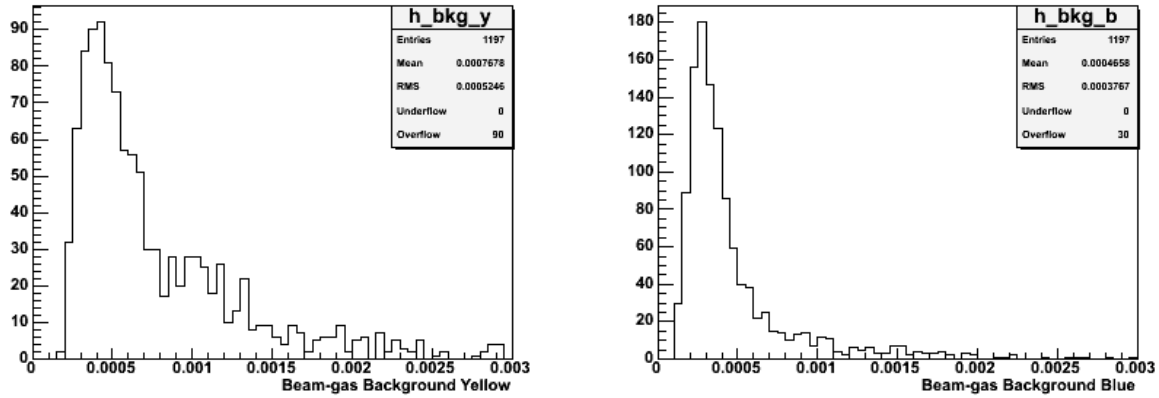

Figure 17: Fraction of the total coincidence rate attributed to beam gas in each beam. The histograms are incremented once for each STAR run.

less than 0.1% of the total rate.

Given run-dependent background fractions for both beams, it's possible to calculate background-subtracted relative luminosities. Figure 18 shows the difference between the raw relative luminosity and the background-subtracted version. The background-corrected relative luminosities yield an A_{LL} that differs from the original by 3.0×10^{-4}, so we use that as the uncertainty for this source of systematic error.

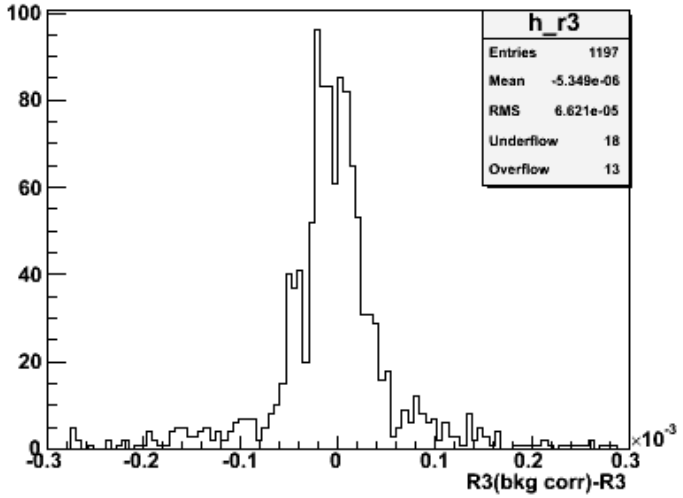

Figure 18: Change in the relative luminosities after correcting for beam-gas background.

A Data Tables

p_T bin	A_{LL}
[2.00 - 3.18]	-0.0055 ± 0.0063 (stat) -0.0062 +0.0034 (syst)
[3.18 - 4.56]	0.0016 ± 0.0099 (stat) -0.0085 +0.0075 (syst)
[4.56 - 6.32]	0.0000 ± 0.0159 (stat) -0.0095 +0.0040 (syst)
[6.32 - 8.80]	-0.0489 ± 0.0264 (stat) -0.0075 +0.0041 (syst)
[8.80 - 12.84]	-0.0330 ± 0.0494 (stat) -0.0052 +0.0061 (syst)

Table 3: π^- Data Table

p_T bin	A_{LL}
[2.00 - 3.18]	-0.0033 ± 0.0061 (stat) -0.0064 +0.0064 (syst)
[3.18 - 4.56]	-0.0015 ± 0.0095 (stat) -0.0130 +0.0069 (syst)
[4.56 - 6.32]	0.0031 ± 0.0152 (stat) -0.0177 +0.0103 (syst)
[6.32 - 8.80]	-0.0019 ± 0.0252 (stat) -0.0210 +0.0187 (syst)
[8.80 - 12.84]	-0.0728 ± 0.0485 (stat) -0.0153 +0.0065 (syst)

Table 4: π^+ Data Table

B Technical Stuff

- Preferred STAR Library: `SL08f`
- Code Repository: `StRoot/StSpinPool/StChargedPionAnalysisMaker`
- HPSS TTree/Histogram Archive: `/home/kocolosk/run5-analysis`
- Relative Luminosities: `StRoot/StSpinPool/StTamuRelLum/input/run5.txt`
- Polarizations: http://www4.rcf.bnl.gov/ cnipol/
- Macro to regenerate TTrees: `macros/RunChargedPion.C`
- Histogramming code: `write_histograms` in `scripts/histos2.py` reads histogram configuration modules in `scripts/config`. The `histos2` module also contains helper functions to automatically distribute the workload using Condor.
- Plotting functions: `scripts/plots/run5note.py`

I'm a big fan of ROOT's Python bindings — all of my analysis code that doesn't directly touch MuDSTs is written in Python. Unfortunately, STAR has not configured its environment to allow us to use PyROOT out-of-the-box, so if you want to regenerate my histograms and plots you need to add:

```
setenv AFS_OPT /afs/rhic.bnl.gov/star/users/kocolosk/public/opt
setenv PYTHONPATH ${AFS_OPT}/lib/python2.3/site-packages:${ROOTSYS}/lib
```

C Runlist

6119032, 6119038, 6119039, 6119063, 6119064, 6119065, 6119066, 6119067, 6119069, 6119071, 6119072, 6120009, 6120010, 6120011, 6120015, 6120016, 6120017, 6120019, 6120022, 6120032, 6120037, 6120038, 6120039, 6120040, 6120042, 6120043, 6120044, 6120045, 6120049, 6120054, 6120066, 6120070, 6120071, 6121009, 6121010, 6121013, 6121014, 6121015, 6121016, 6121018, 6121021, 6121022, 6121033, 6121036, 6121060, 6121061, 6121068, 6121070, 6121071, 6121072, 6121073, 6121075, 6121076, 6122001, 6122002, 6122010, 6122011, 6122013, 6122014, 6122018, 6127035, 6127036, 6127037, 6128005, 6128006, 6128007, 6128009, 6128011, 6128012, 6128013, 6128014, 6128015, 6128016, 6128022, 6128023, 6128024, 6128026, 6128027, 6128028, 6128029, 6128030, 6128031, 6128032, 6131007, 6131008, 6131009, 6131013, 6131048, 6131049, 6131052, 6131053, 6131054, 6131056, 6131057, 6131092, 6133006, 6133009, 6133010, 6133011, 6133012, 6133013, 6133014, 6133015, 6133016, 6133017, 6133018, 6133022, 6133026, 6133049, 6133071, 6133072, 6134001, 6134002, 6134003, 6134004, 6134005, 6134006, 6134007, 6134008, 6134010, 6134011, 6134024, 6134047, 6134060, 6136014, 6136015, 6136017, 6136018, 6136028, 6136029, 6136030, 6136031, 6136032, 6136034, 6136035, 6136037, 6136041, 6136042, 6136043, 6136119, 6136130, 6136131, 6137009, 6137011, 6137149, 6137157, 6137158, 6137159, 6137160, 6137163, 6137164, 6137166, 6137167, 6137169, 6137170, 6137171, 6137172, 6137173, 6138001, 6138002, 6138003, 6138004, 6138005, 6138010, 6138011, 6138012, 6138013, 6138014, 6138017, 6138018, 6138019, 6138020, 6138059, 6138061, 6138062, 6138067, 6139001, 6139002, 6139004, 6139005, 6139007, 6139008, 6139009, 6139010, 6139012, 6139013, 6139018, 6139019, 6139020, 6139021, 6139022, 6139025, 6139026, 6139027, 6139028, 6139029, 6139030, 6139034, 6139036, 6139039, 6139041, 6139054, 6139055, 6139056, 6139061, 6139063, 6139064, 6139065, 6139071, 6140002, 6140003, 6140004, 6140005, 6140018, 6140019, 6140020, 6140021, 6140022, 6140023, 6140024, 6140025, 6140026, 6140028, 6140029, 6140030, 6140031, 6140032, 6140033, 6140034, 6140035, 6140036, 6140054, 6140065, 6140066, 6140067, 6140068, 6140069, 6140074, 6140075, 6140076, 6141009, 6141010, 6141011, 6141021, 6141022, 6141023, 6141026, 6141027, 6141028, 6141029, 6141030, 6141031, 6141032,

6141033, 6141047, 6141049, 6141050, 6141051, 6141052, 6141053, 6141058, 6141061, 6141062, 6141063, 6141064, 6141065, 6141066, 6141068, 6141069, 6142001, 6142002, 6142003, 6142004, 6142005, 6142006, 6142007, 6142008, 6142010, 6142011, 6142012, 6142013, 6142014, 6142015, 6142016, 6142017, 6142018, 6142020, 6142021, 6142022, 6142024, 6142025, 6142026, 6142027, 6142077, 6142078, 6142079, 6142080, 6142081, 6142082, 6142084, 6142087, 6142088, 6142089, 6142093, 6142094, 6142097, 6143001, 6143002, 6143012, 6143013, 6143014, 6143015, 6143016, 6143017, 6143018, 6143019, 6143021, 6143022, 6143023, 6143024, 6143025, 6143027, 6143028, 6143033, 6144017, 6144019, 6144020, 6144021, 6144022, 6144023, 6144024, 6144026, 6144028, 6144051, 6144052, 6144053, 6144054, 6144057, 6144058, 6144059, 6144060, 6144061, 6144063, 6144066, 6144067, 6145011, 6145013, 6145015, 6145018, 6145019, 6145020, 6145023, 6145025, 6145027, 6145028, 6145041, 6145045, 6145053, 6145054, 6145055, 6145056, 6145057, 6145058, 6145068, 6146017, 6146018, 6146019, 6146020, 6146021, 6146024, 6146025, 6147009, 6147029, 6147030, 6147031, 6148008, 6148009, 6148010, 6148011, 6148012, 6148013, 6148014, 6148017, 6148018, 6148019, 6148020, 6148021, 6148022, 6148024, 6148026, 6148027, 6148037, 6148040, 6148041, 6148054, 6148055, 6148056, 6148057, 6148058, 6148059, 6148060, 6148063, 6148064, 6149003, 6149004, 6149007, 6149009, 6149016, 6149017, 6149018, 6149019, 6149020, 6149021, 6149024, 6149025, 6149029, 6149030, 6149031, 6149032, 6149036, 6149048, 6149050, 6149051, 6149052, 6149055, 6149056, 6149057, 6150005, 6150006, 6150014, 6150015, 6150016, 6150017, 6150018, 6150019, 6150022, 6150023, 6150024, 6150025, 6150026, 6150027, 6150028, 6150029, 6150037, 6150038, 6151001, 6151002, 6151005, 6151008, 6151009, 6151011, 6151012, 6151013, 6151014, 6151015, 6151017, 6151018, 6151020, 6151021, 6151022, 6151023, 6151024, 6151026, 6151028, 6151029, 6151030, 6155004, 6155026, 6155027, 6155029, 6156004, 6156010, 6156011, 6156012, 6156013, 6156014, 6156015, 6156016, 6156019, 6156027, 6156028, 6156029, 6156030, 6156034, 6156036, 6157050, 6157051, 6158014, 6158015, 6158019, 6158020, 6158024, 6158025, 6158041, 6158057, 6158059, 6158060, 6158061, 6158062, 6158063, 6158076, 6158077, 6158081, 6158084, 6158085, 6158086, 6160039, 6160040, 6160041, 6160044, 6160048, 6160056, 6160057, 6160058, 6160061, 6160062, 6160065, 6160068, 6160069, 6160070, 6160071, 6160072, 6160082, 6160083, 6161001, 6161006, 6161007, 6161035, 6161038, 6161042, 6161043, 6161044, 6161046, 6161047, 6161091, 6161092, 6161093, 6161094, 6161097, 6161098, 6161099, 6161100, 6161101, 6161102, 6161104, 6161105, 6162005, 6162006, 6162007, 6162014, 6162027, 6162028, 6162029, 6162030, 6162031, 6162032, 6162039, 6162040, 6162041, 6162042, 6162043, 6162044, 6162045, 6162046, 6162056, 6162058, 6162061, 6162062, 6162063, 6162064, 6162068, 6162069, 6162070, 6162071, 6162072, 6162075, 6162076, 6163012, 6163013, 6163015, 6163016, 6163017, 6163018, 6163021, 6163022, 6163023, 6163024, 6163025, 6163035, 6163038, 6163039, 6163040, 6163041, 6163043,

6163044, 6163045, 6163048, 6163050, 6163051, 6163053, 6163054, 6163056, 6163057, 6163058, 6164002, 6164003, 6164004, 6164013, 6164016, 6164017, 6164018, 6164021, 6164022, 6164023, 6164024, 6167115, 6167116, 6167119, 6167131, 6167134, 6167140, 6167141, 6168002, 6168018, 6168019, 6168022, 6168023, 6168024, 6168036, 6168044, 6168068, 6168069, 6168072, 6168073, 6168083, 6168084, 6168085, 6168086, 6168089, 6168090, 6168099, 6168100, 6168101, 6168102, 6168103, 6168104, 6168107, 6168108, 6168111, 6168112, 6169001, 6169002, 6169003, 6169006, 6169007, 6169008, 6169020, 6169025, 6169026, 6169027, 6169028, 6169029, 6169030, 6169031, 6169035, 6169036, 6169037, 6169038, 6169039, 6169041, 6169043, 6169044, 6169047, 6169048, 6169049, 6169050, 6169051, 6169052, 6169053, 6169055, 6169056, 6169057, 6169058, 6169060, 6169073, 6169079, 6169080, 6169082, 6169083, 6169084, 6169088, 6169089, 6169090, 6169091, 6169092, 6169093, 6169094, 6169096, 6169097, 6169101, 6169103, 6169104, 6169105, 6169106, 6169107, 6170002, 6170006, 6170009, 6170010, 6170011, 6170012, 6170013, 6170014, 6170015, 6170016, 6170017, 6170018, 6170031, 6170032, 6170033, 6170034, 6170035, 6170038, 6170039, 6170040, 6170041, 6170045, 6171022, 6171024, 6171034, 6171039, 6171040, 6171041, 6171043, 6171044, 6171045, 6171046, 6171048, 6171049, 6171062, 6171063, 6172001, 6172002, 6172003, 6172006, 6172007, 6172010, 6172015, 6172016, 6172069, 6172085, 6172086, 6172087, 6172092, 6172093, 6174010, 6174011, 6174012, 6174013, 6174014, 6174017, 6174018, 6174019, 6174020, 6174021, 6174025, 6174026, 6174027, 6174031, 6174044, 6174045, 6174046, 6174047, 6174048, 6174049, 6174053, 6174054, 6174055, 6174056, 6174057, 6174058, 6174059, 6174060, 6174069, 6174070, 6174072

D PID Fits

The following pages display fit results used to determine optimal $n\sigma(\pi)$ integration windows and background fractions.

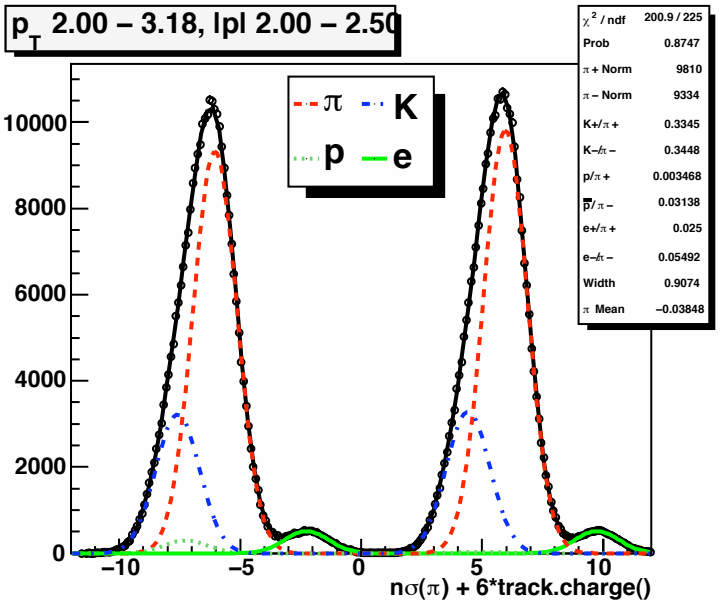

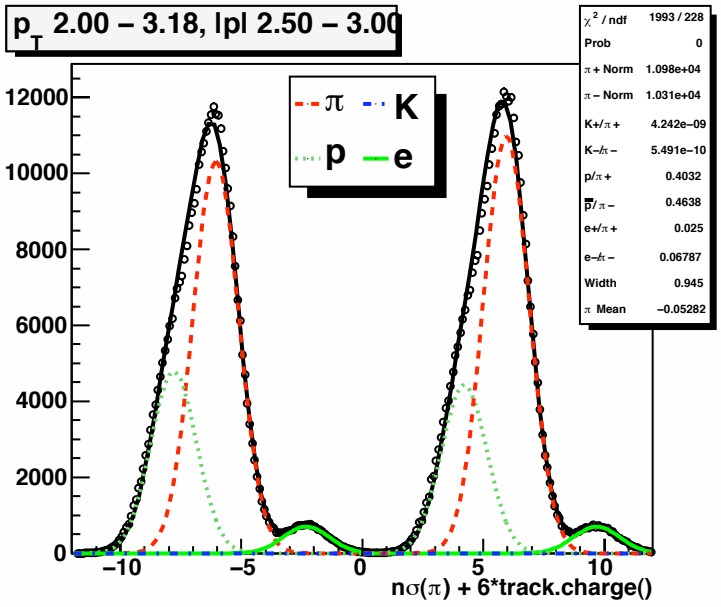

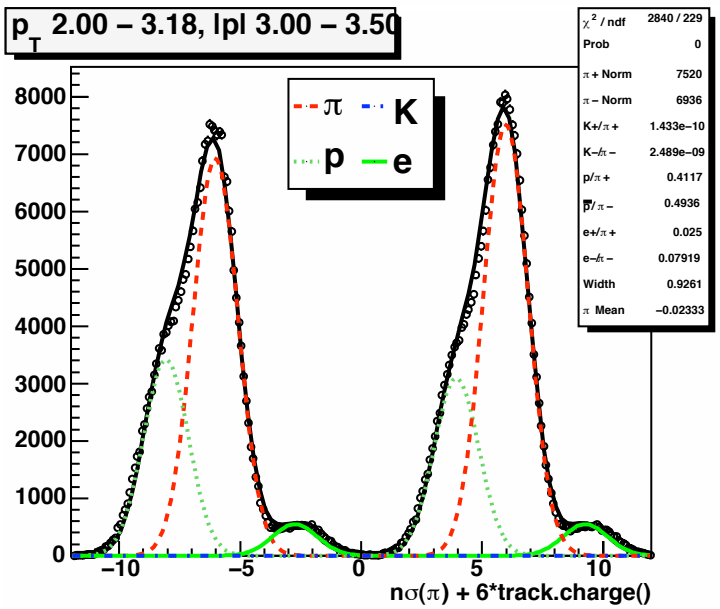

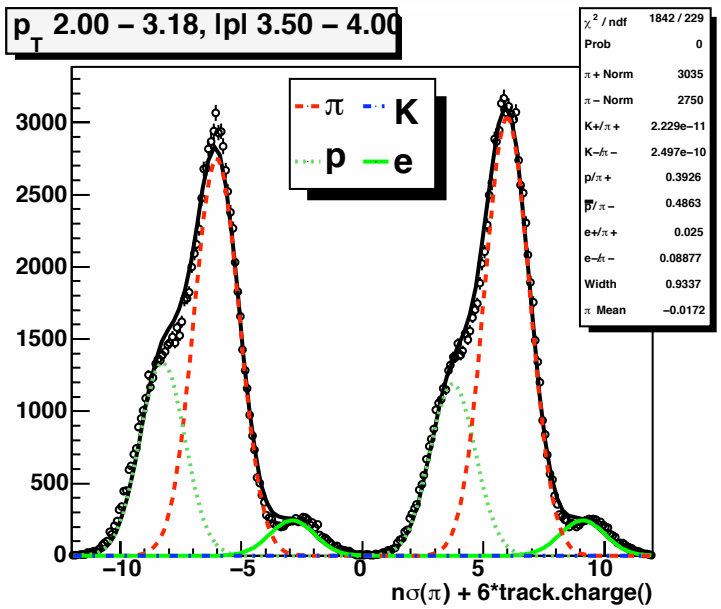

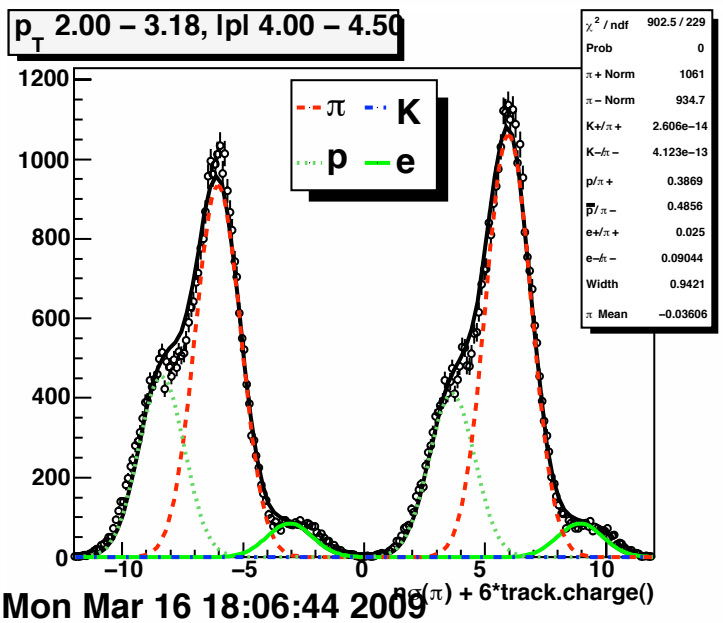

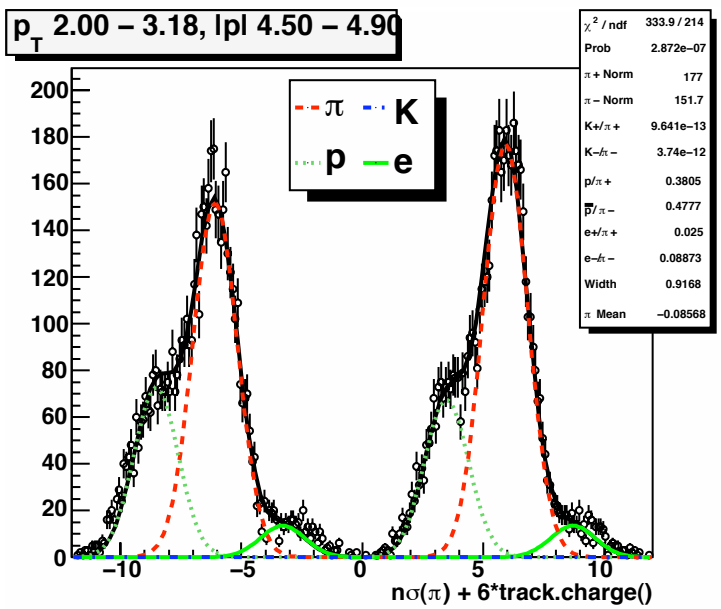

Mon Mar 16 18:06:44 2009

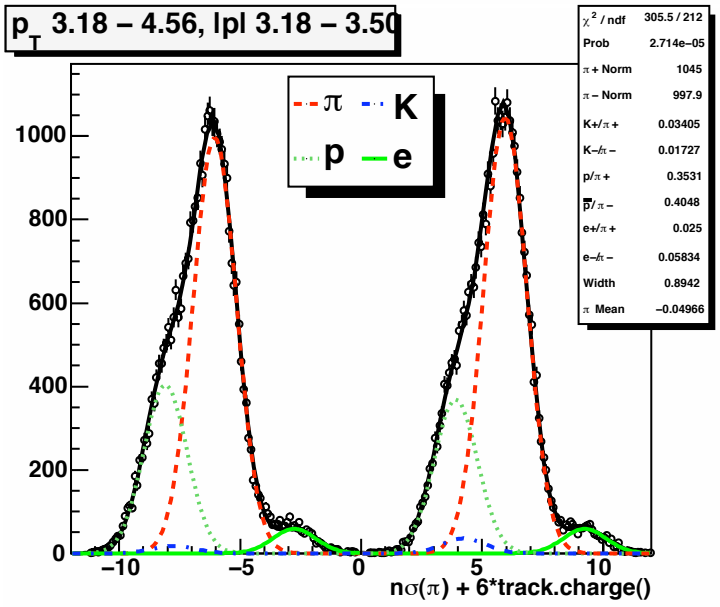

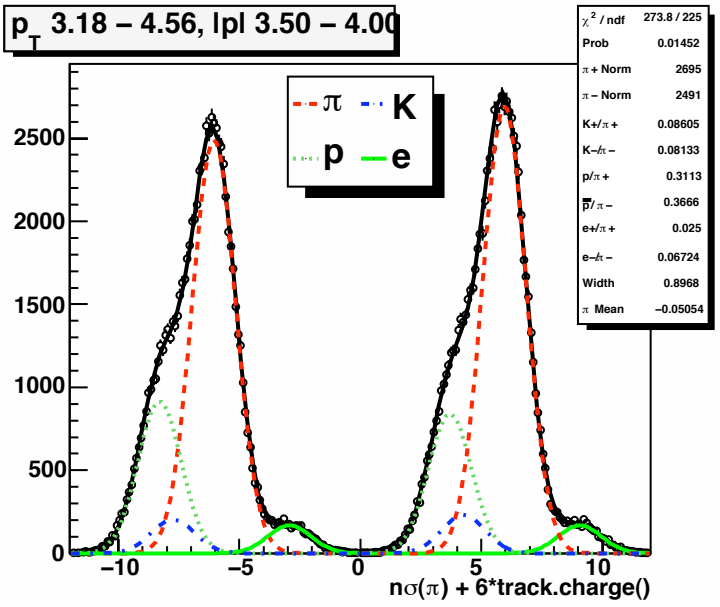

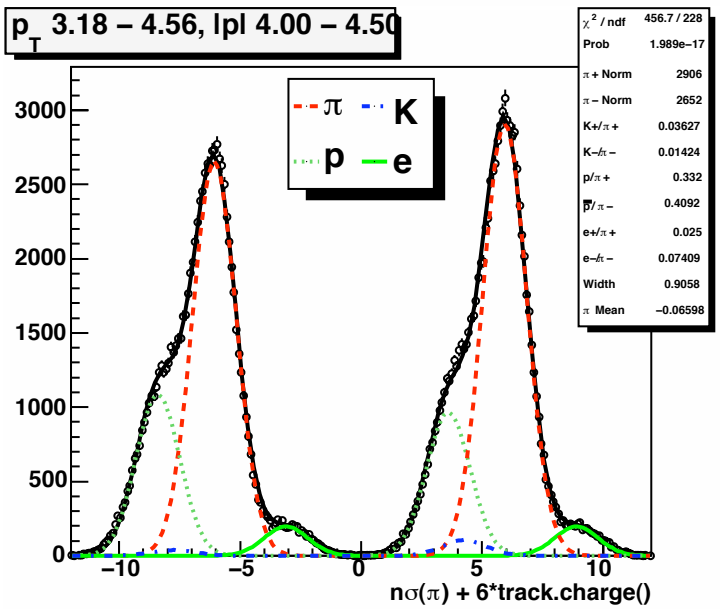

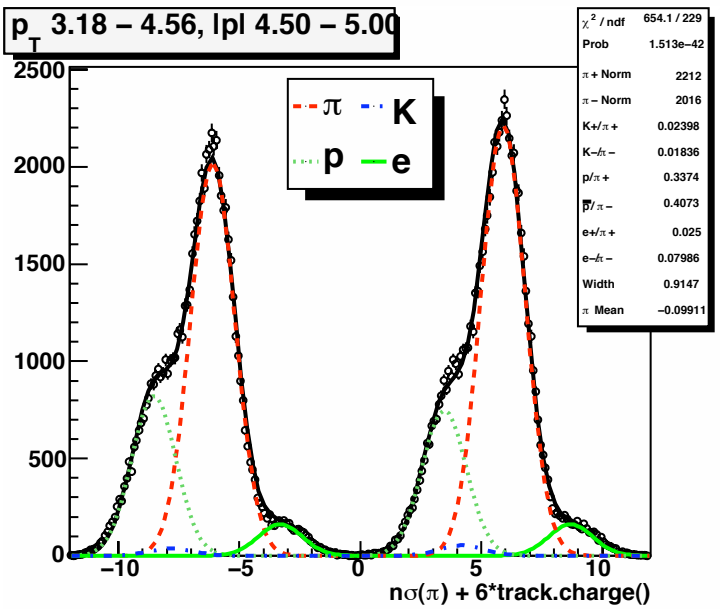

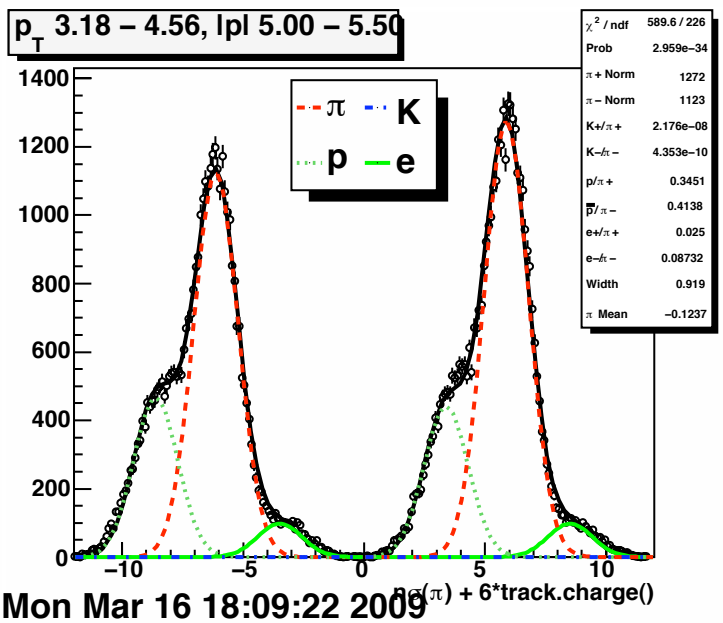

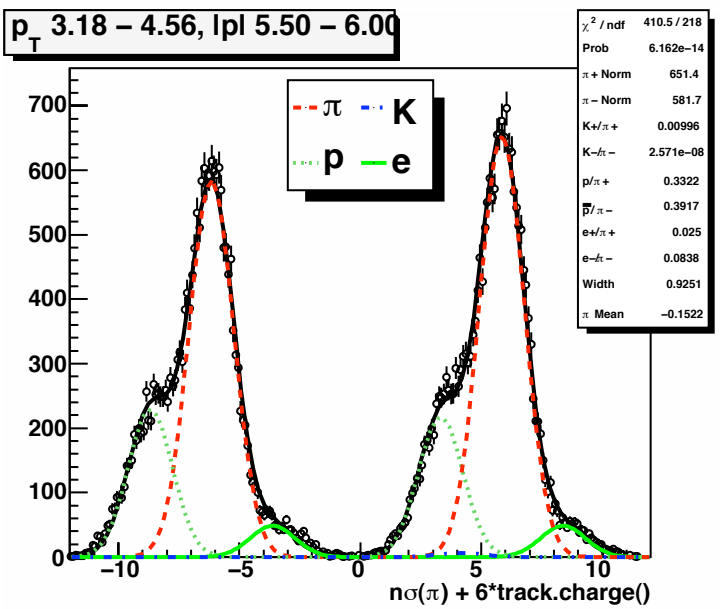

Mon Mar 16 18:09:22 2009

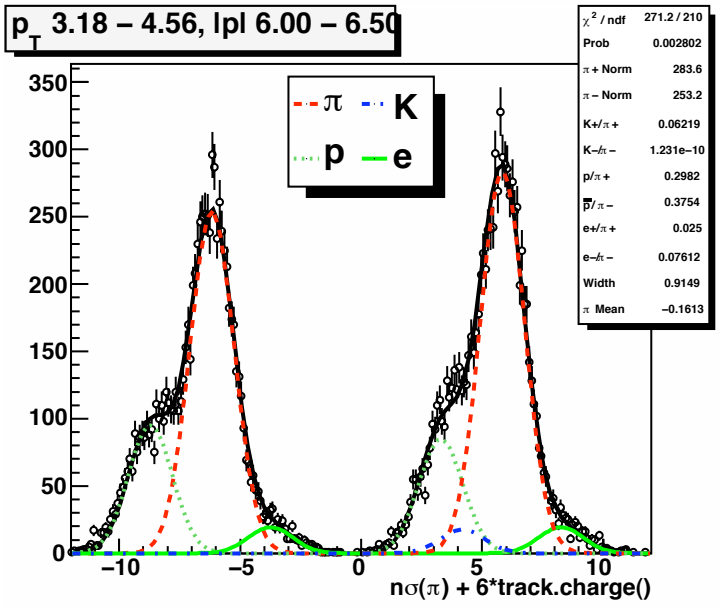

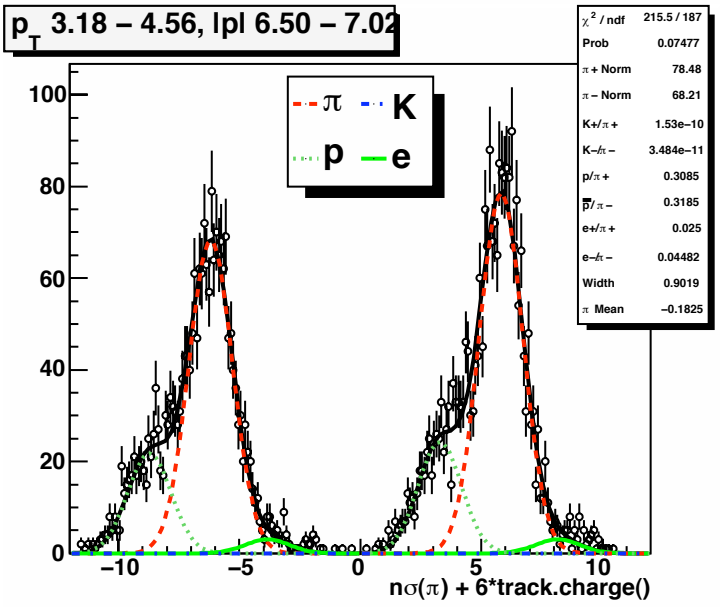

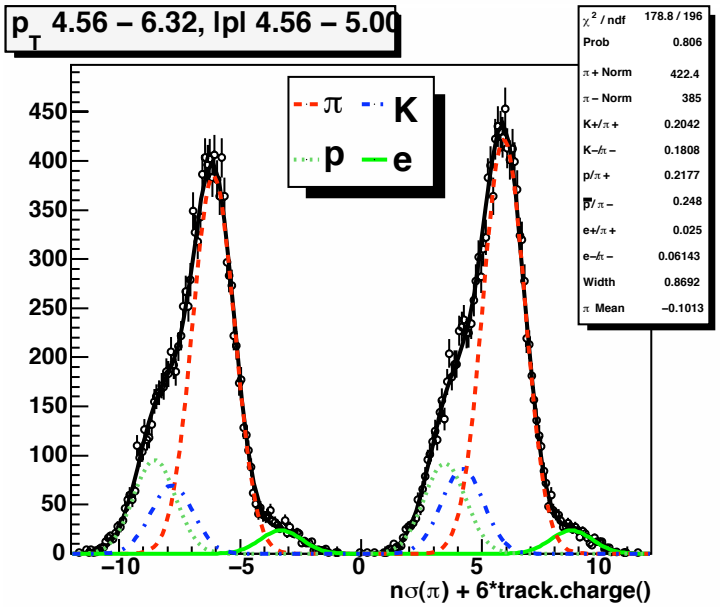

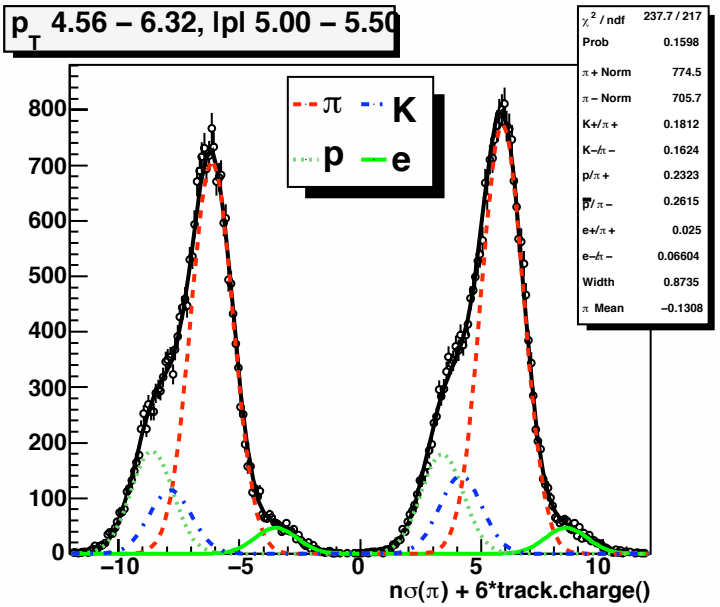

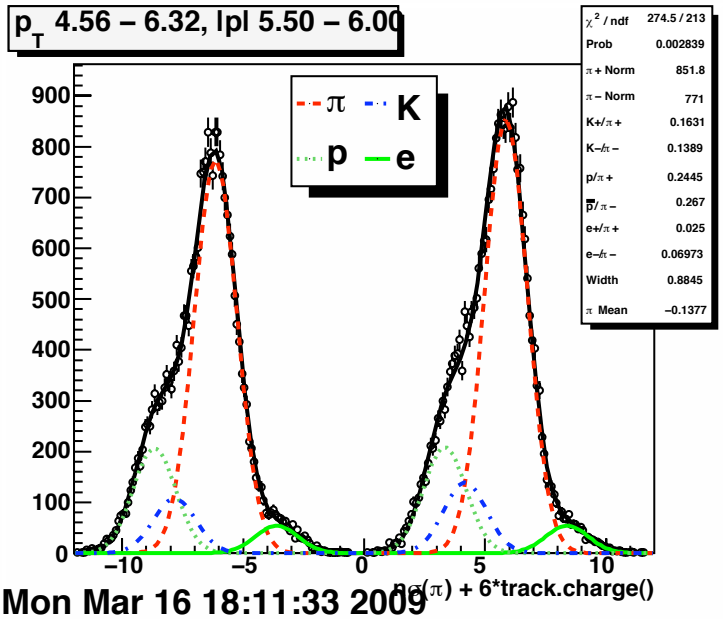

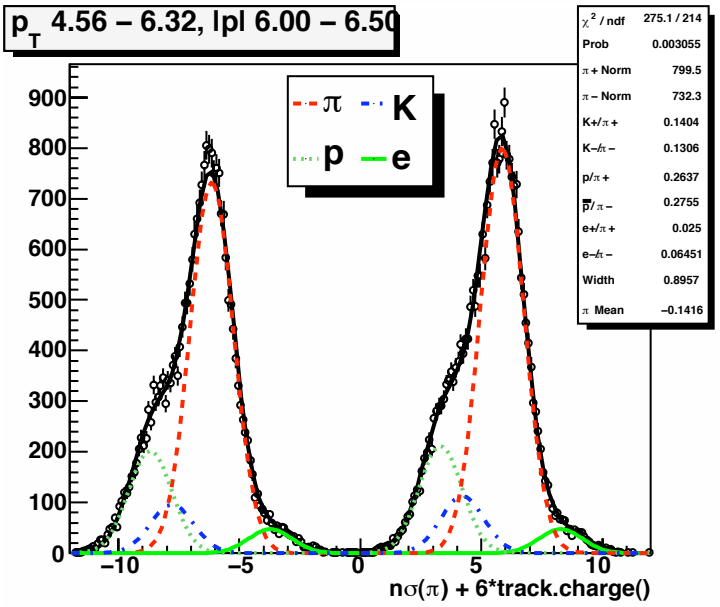

Mon Mar 16 18:11:33 2009

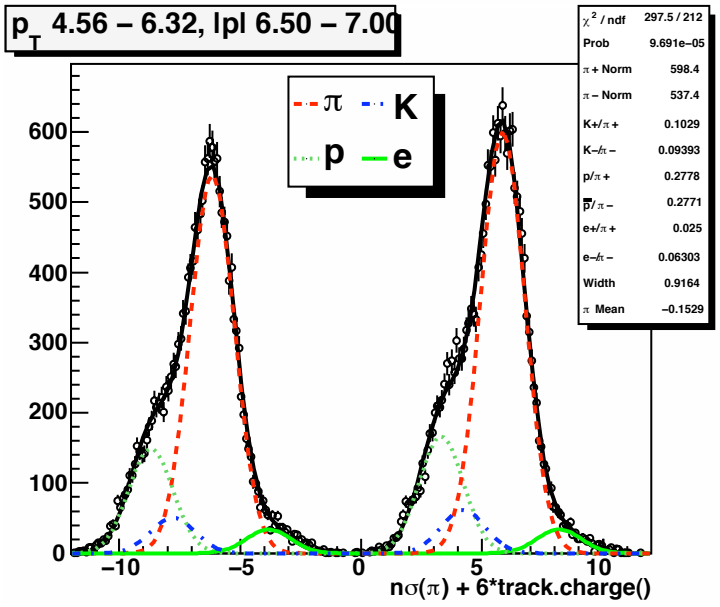

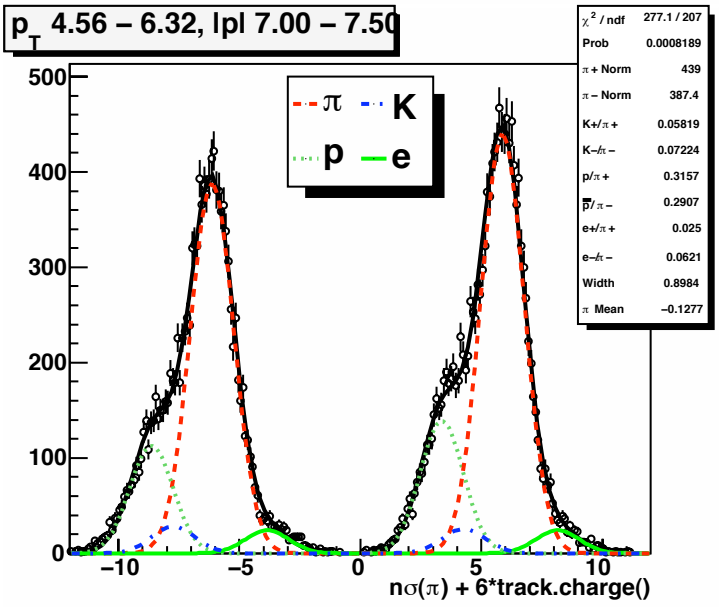

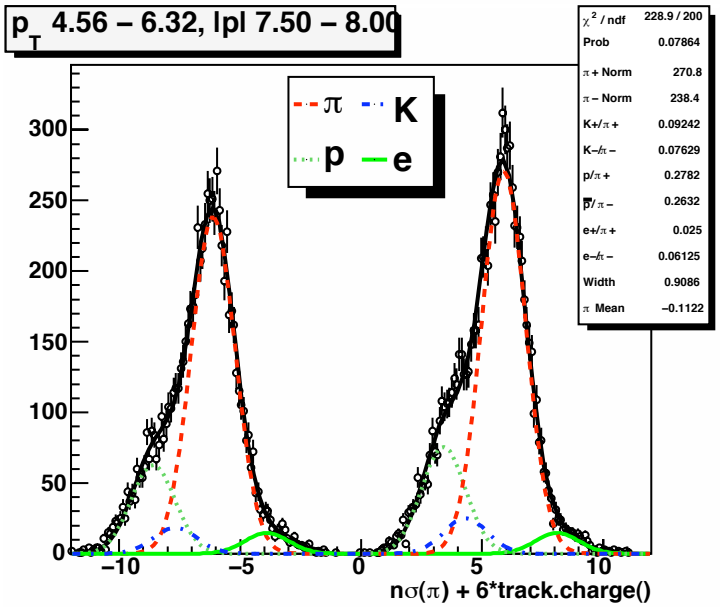

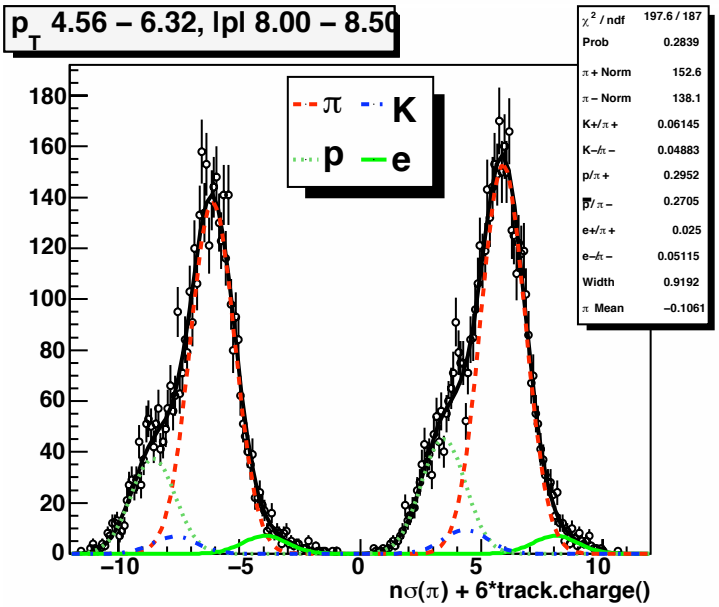

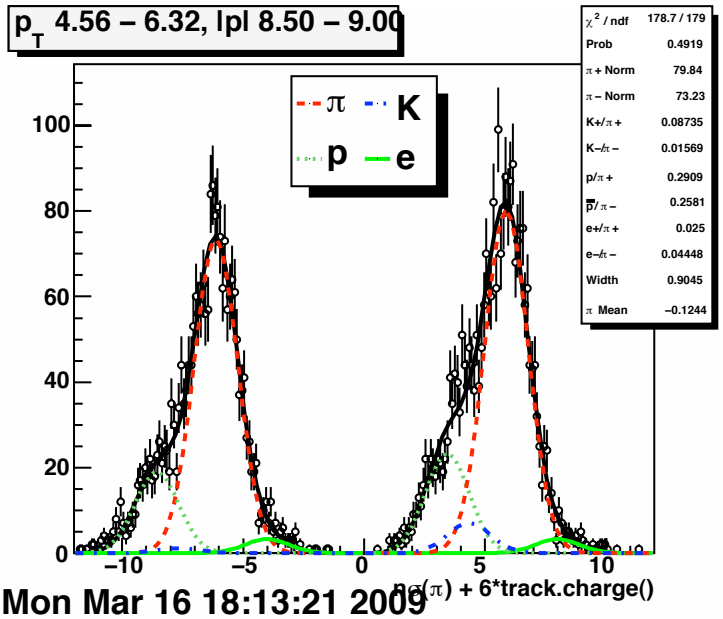

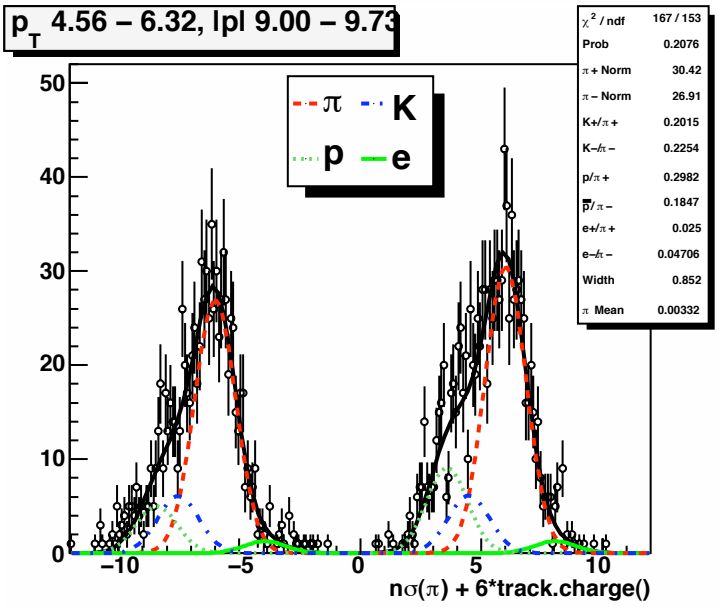

Mon Mar 16 18:13:21 2009

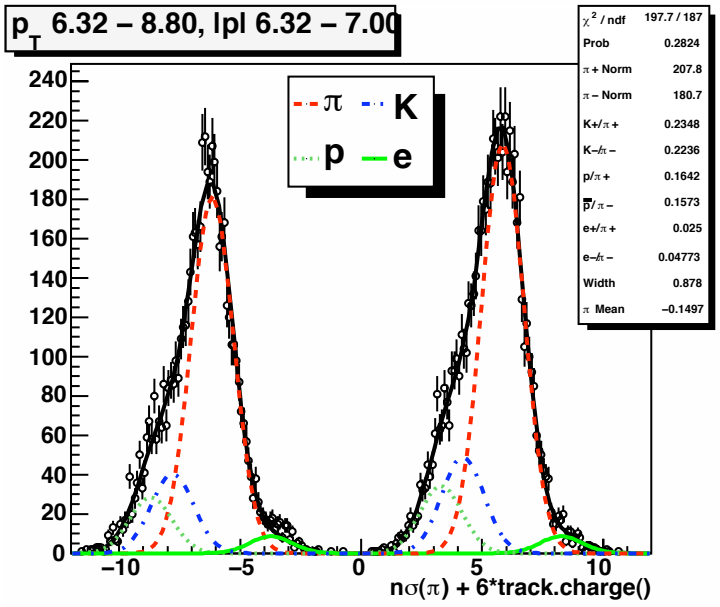

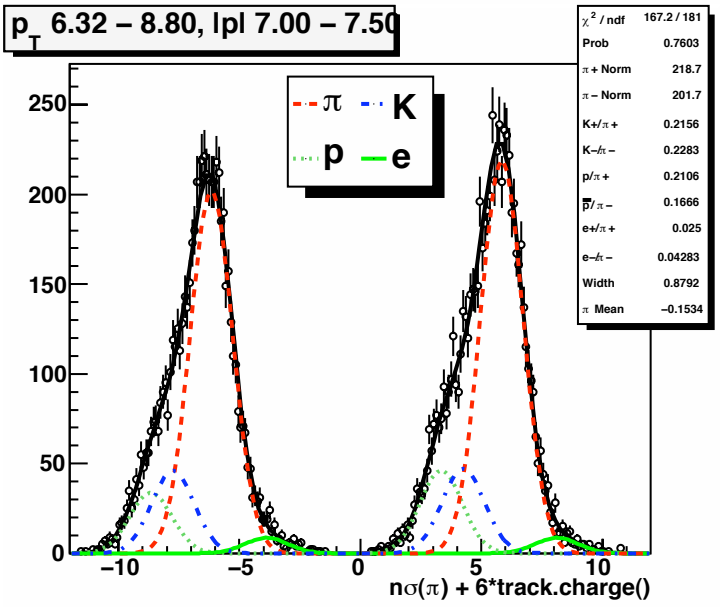

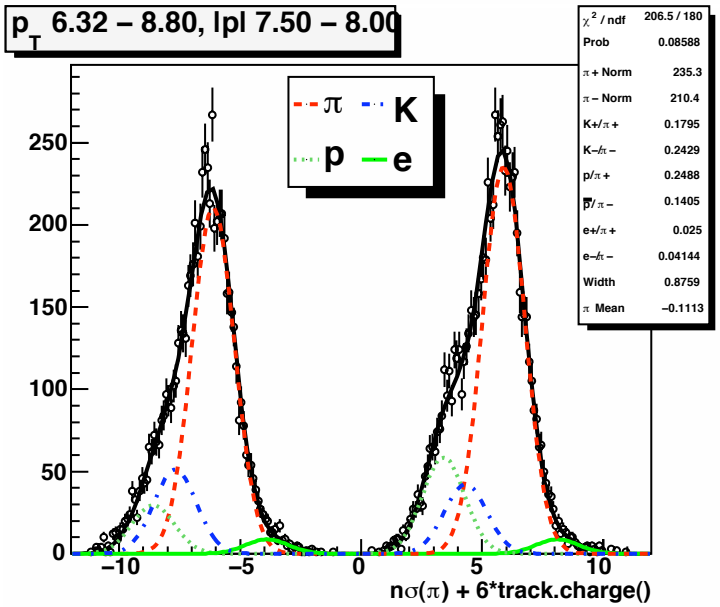

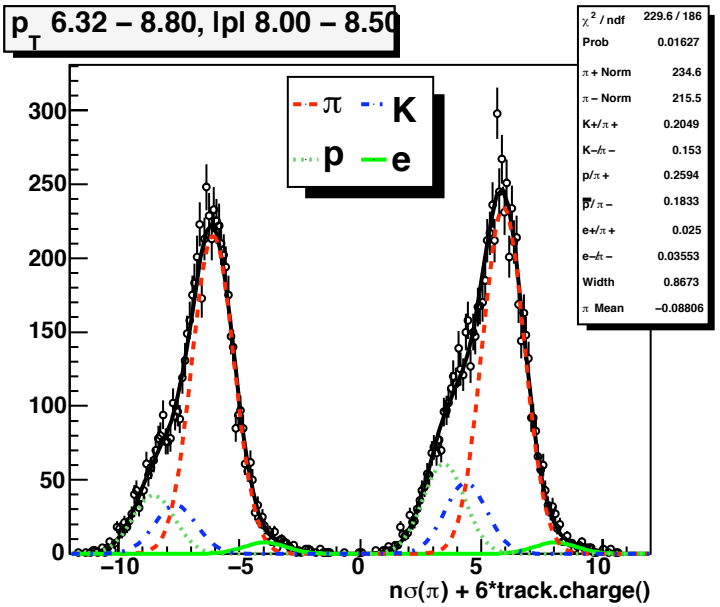

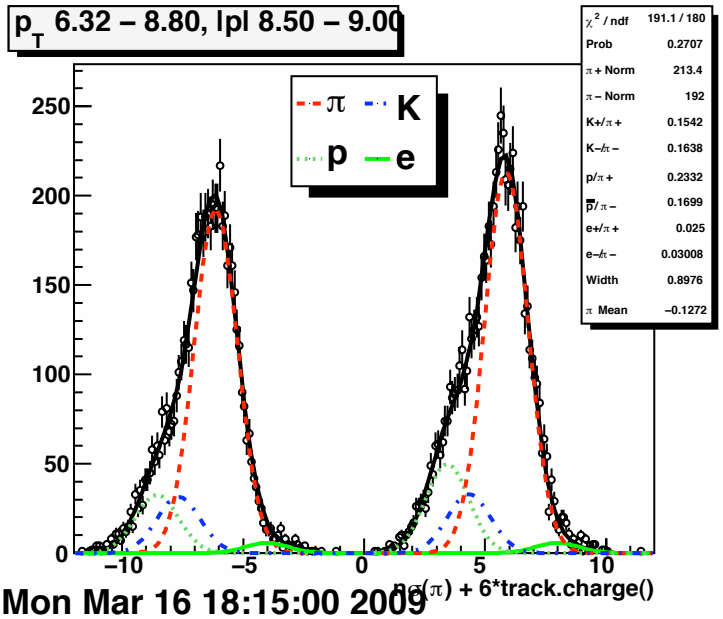

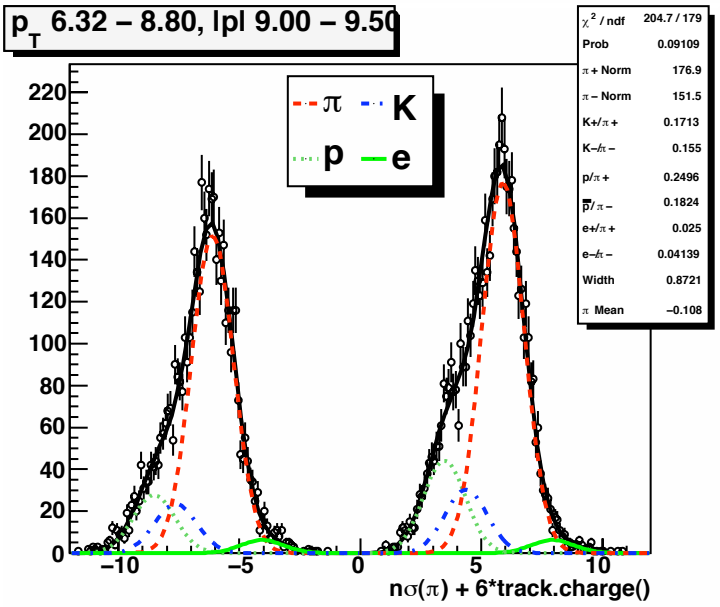

Mon Mar 16 18:15:00 2009

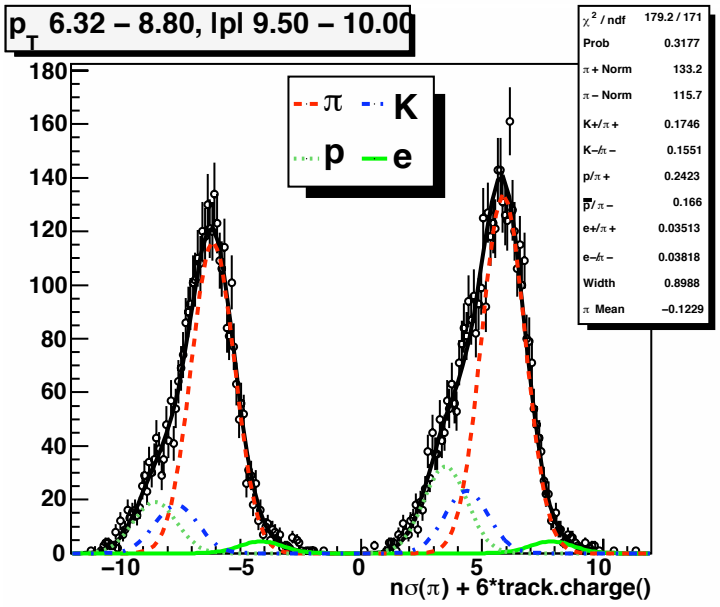

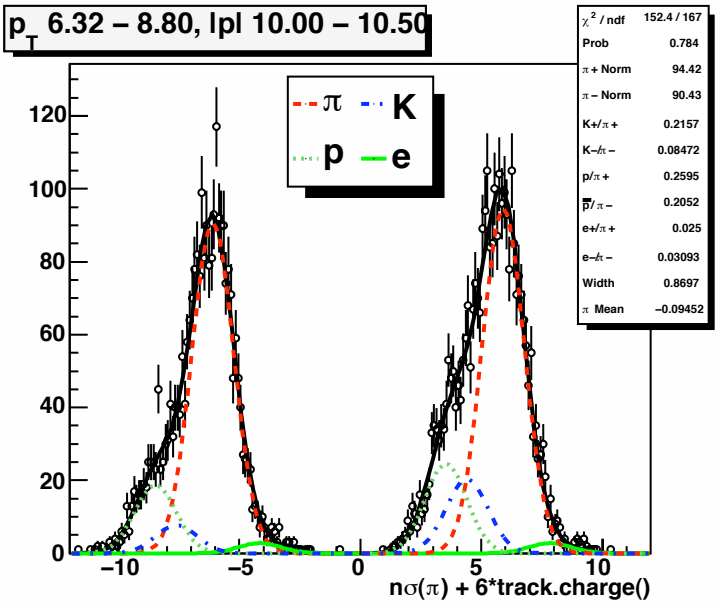

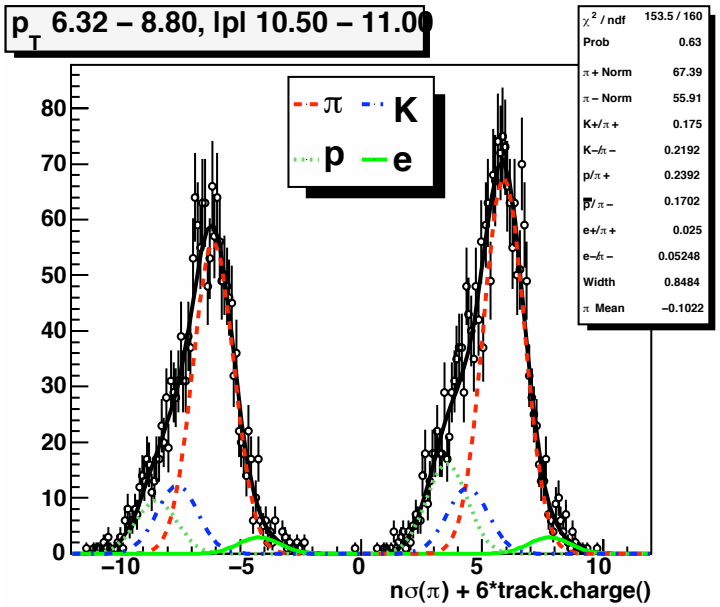

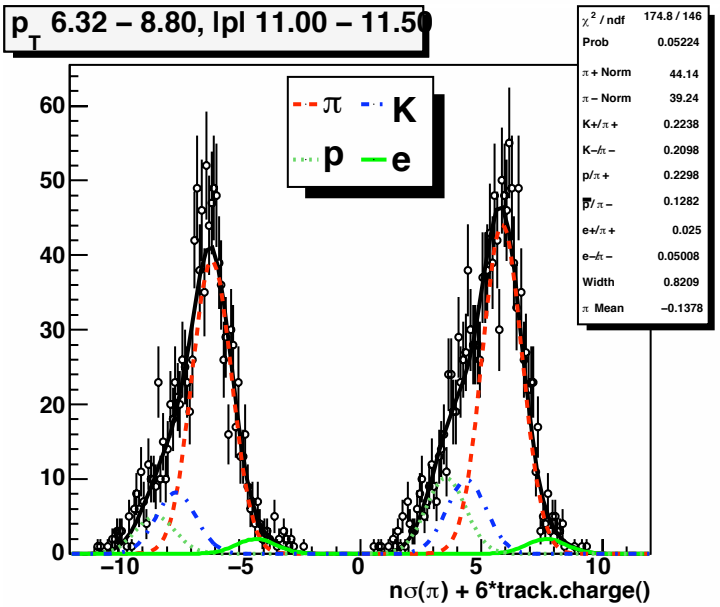

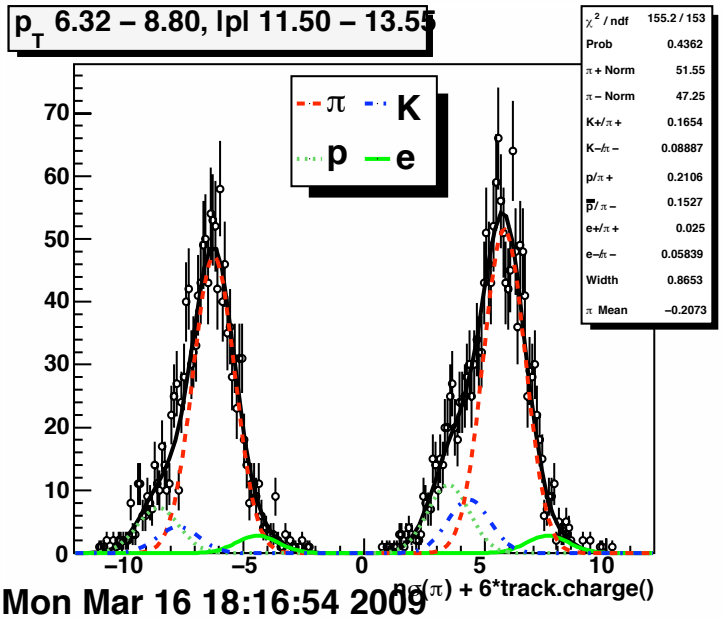

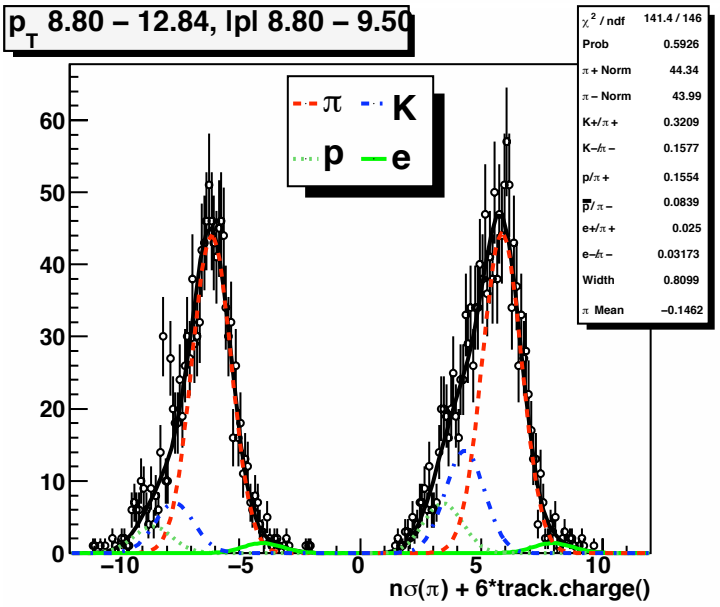

Mon Mar 16 18:16:54 2009

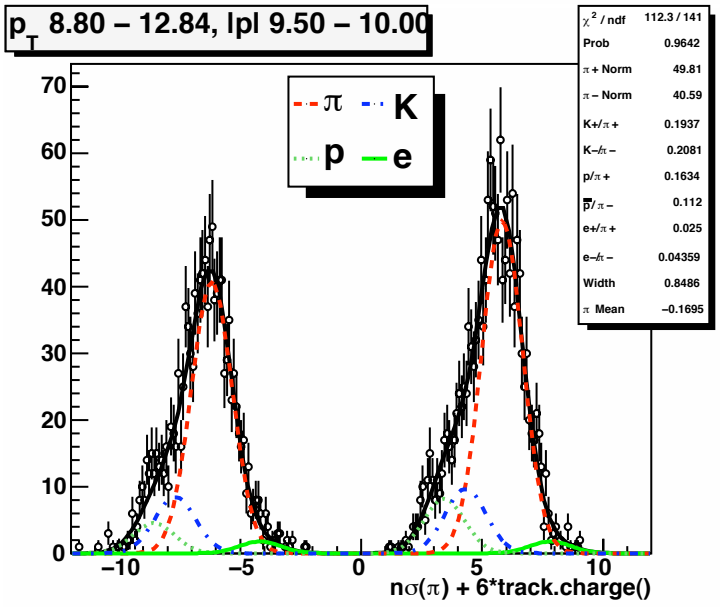

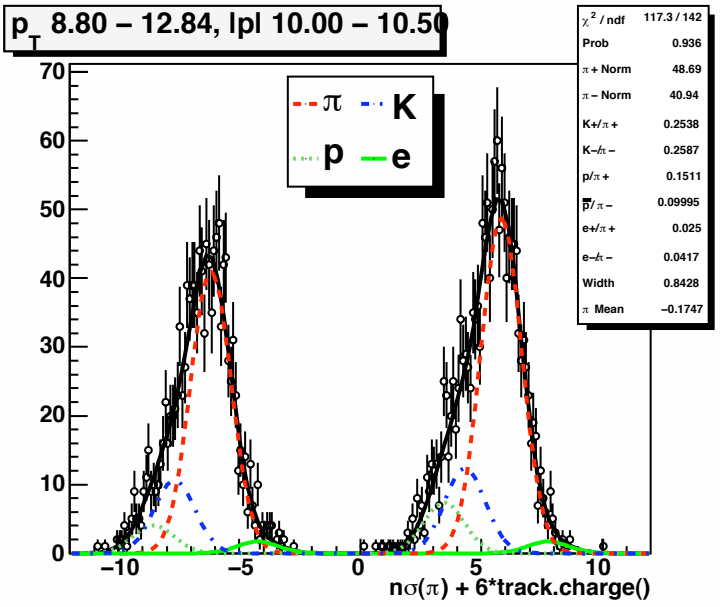

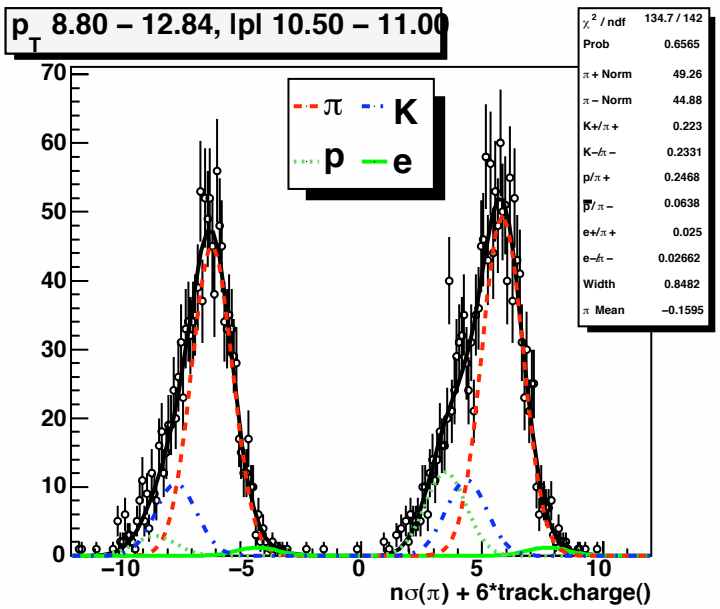

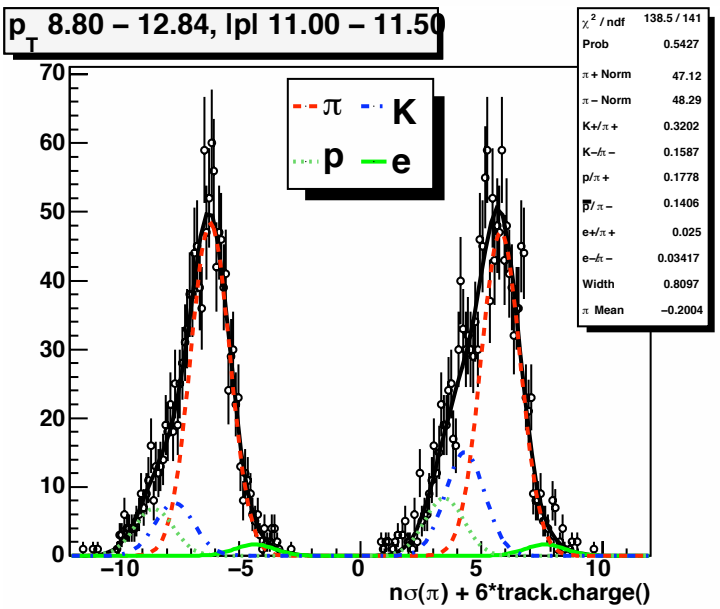

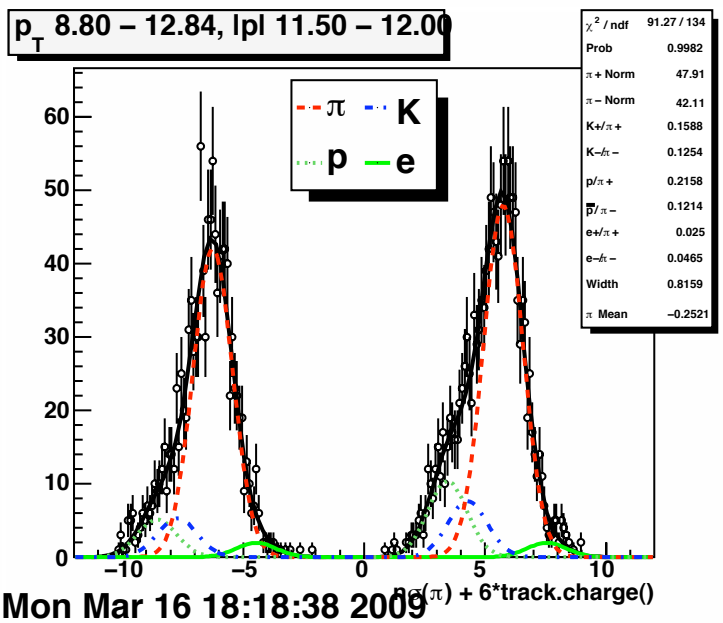

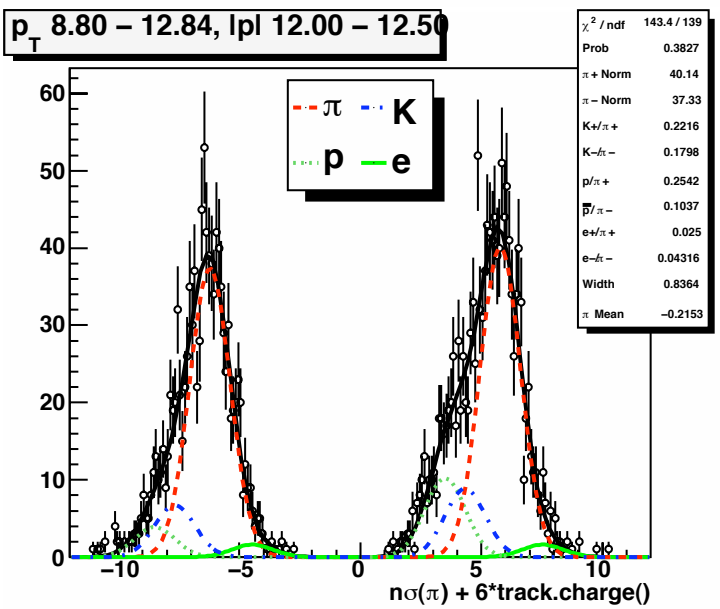

Mon Mar 16 18:18:38 2009

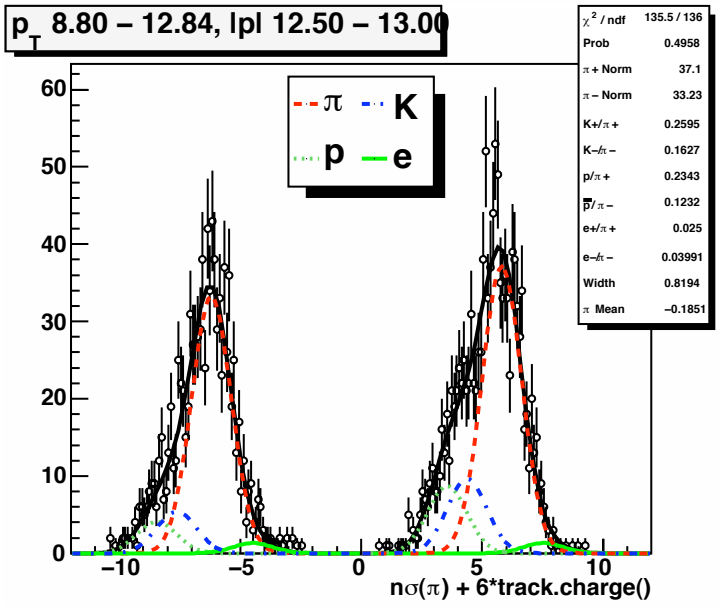
p_T 8.80 – 12.84, lpl 12.50 – 13.00
π K p e
χ^2 / ndf 135.5 / 136
Prob 0.4958
π + Norm 37.1
π – Norm 33.23
K+/π + 0.2595
K–/π – 0.1627
p/π + 0.2343
$\bar{p}$/π – 0.1232
e+/π + 0.025
e–/π – 0.03991
Width 0.8194
π Mean –0.1851
nσ(π) + 6*track.charge()

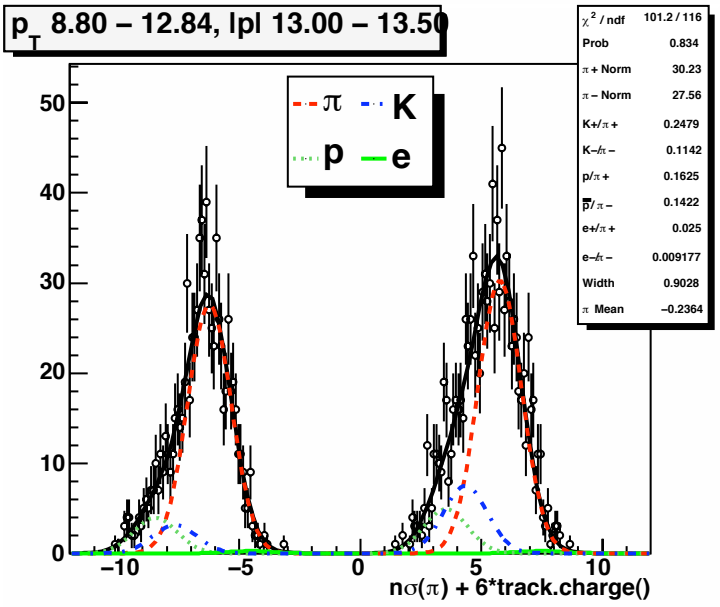
p_T 8.80 – 12.84, lpl 13.00 – 13.50
π K p e
χ^2 / ndf 101.2 / 116
Prob 0.834
π + Norm 30.23
π – Norm 27.56
K+/π + 0.2479
K–/π – 0.1142
p/π + 0.1625
$\bar{p}$/π – 0.1422
e+/π + 0.025
e–/π – 0.009177
Width 0.9028
π Mean –0.2364
nσ(π) + 6*track.charge()

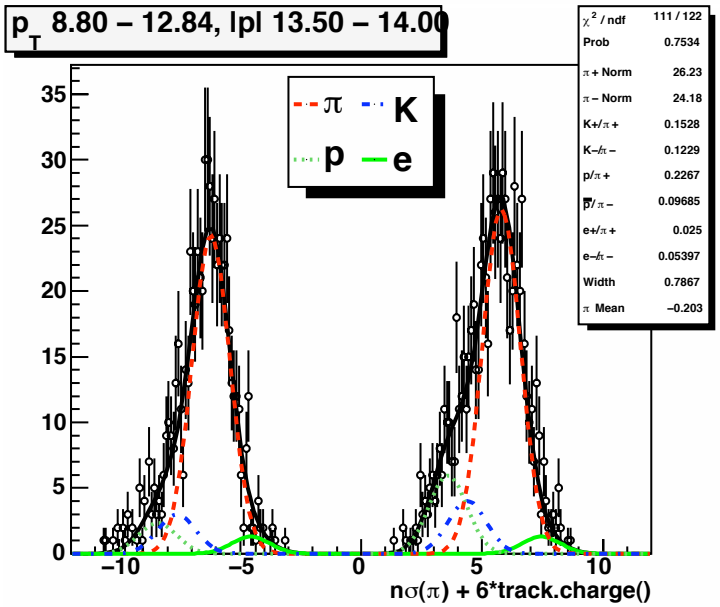
p_T 8.80 – 12.84, lpl 13.50 – 14.00
π K p e
χ^2 / ndf 111 / 122
Prob 0.7534
π + Norm 26.23
π – Norm 24.18
K+/π + 0.1528
K–/π – 0.1229
p/π + 0.2267
$\bar{p}$/π – 0.09685
e+/π + 0.025
e–/π – 0.05397
Width 0.7867
π Mean –0.203
nσ(π) + 6*track.charge()

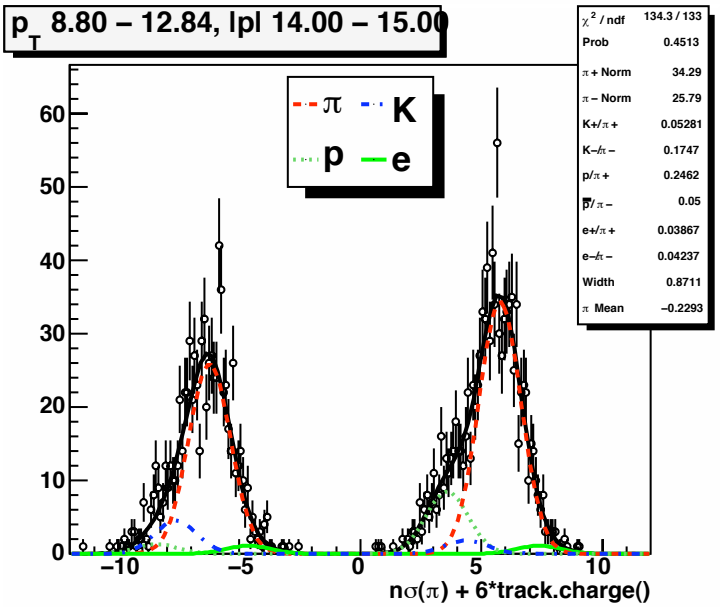
p_T 8.80 – 12.84, lpl 14.00 – 15.00
π K p e
χ^2 / ndf 134.3 / 133
Prob 0.4513
π + Norm 34.29
π – Norm 25.79
K+/π + 0.05281
K–/π – 0.1747
p/π + 0.2462
$\bar{p}$/π – 0.05
e+/π + 0.03867
e–/π – 0.04237
Width 0.8711
π Mean –0.2293
nσ(π) + 6*track.charge()

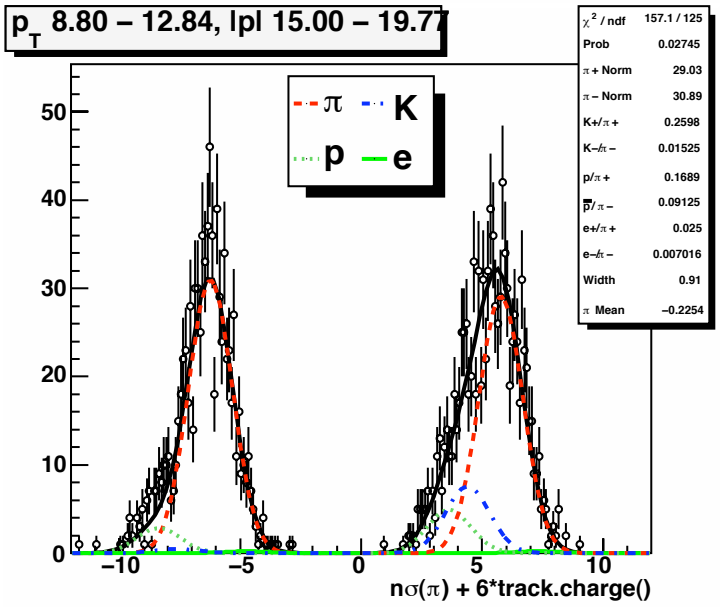
p_T 8.80 – 12.84, lpl 15.00 – 19.77
π K p e
χ^2 / ndf 157.1 / 125
Prob 0.02745
π + Norm 29.03
π – Norm 30.89
K+/π + 0.2598
K–/π – 0.01525
p/π + 0.1689
$\bar{p}$/π – 0.09125
e+/π + 0.025
e–/π – 0.007016
Width 0.91
π Mean –0.2254
nσ(π) + 6*track.charge()